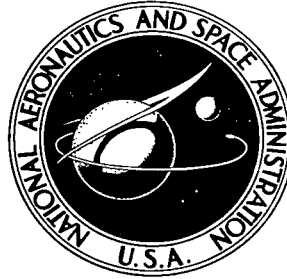


NASA TECHNICAL NOTE



NASA TN D-8383 *2.1*

NASA TN D-8383

LOAN COPY: RET
AFWL TECHNICAL
KIRTLAND AFB



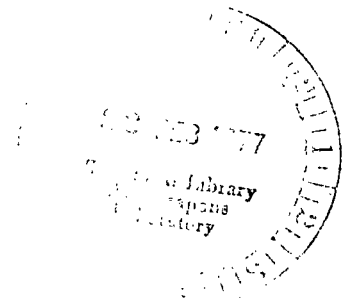
REACTION DIFFUSION
IN THE NICKEL-CHROMIUM-ALUMINUM
AND COBALT-CHROMIUM-ALUMINUM SYSTEMS

Stanley R. Levine

Lewis Research Center

and U.S. Army Air Mobility R&D Laboratory

Cleveland, Ohio 44135





0134090

1. Report No. NASA TN D-8383	2. Government Accession No.	3. Recipient's Catalog No.	
4. Title and Subtitle REACTION DIFFUSION IN THE NICKEL-CHROMIUM-ALUMINUM AND COBALT-CHROMIUM-ALUMINUM SYSTEMS		5. Report Date February 1977	6. Performing Organization Code
7. Author(s) Stanley R. Levine		8. Performing Organization Report No. E-8835	10. Work Unit No. 505-01
9. Performing Organization Name and Address NASA Lewis Research Center and U.S. Army Air Mobility R & D Laboratory Cleveland, Ohio 44135		11. Contract or Grant No.	13. Type of Report and Period Covered Technical Note
12. Sponsoring Agency Name and Address National Aeronautics and Space Administration Washington, D. C. 20546		14. Sponsoring Agency Code	
15. Supplementary Notes			
16. Abstract The effects of MCrAl coating-substrate interdiffusion on oxidation life and the general multi-phase, multicomponent diffusion problem were examined. Semi-infinite diffusion couples that had sources representing coatings and sinks representing gas turbine alloys were annealed at 1000 ^o , 1095 ^o , 1150 ^o , or 1205 ^o C for as long as 500 hours. The source and sink aluminum and chromium contents and the base metal (cobalt or nickel) determined the parabolic diffusion rate constants of the couples and predicted finite coating lives. The β source strength concept provided a method (1) for correlating β recession rate constants with composition; (2) for determining reliable average total, diffusion, and constitutional activation energies; and (3) for calculating interdiffusion coefficients.			
17. Key Words (Suggested by Author(s)) Diffusion; Nickel alloys; Cobalt alloys; Protective coatings; Gas turbines		18. Distribution Statement Unclassified - unlimited STAR Category 26	
19. Security Classif. (of this report) Unclassified	20. Security Classif. (of this page) Unclassified	21. No. of Pages 66	22. Price* A04

REACTION DIFFUSION IN THE NICKEL-CHROMIUM-ALUMINUM AND COBALT-CHROMIUM-ALUMINUM SYSTEMS

by Stanley R. Levine

Lewis Research Center and
U. S. Army Air Mobility R&D Laboratory

SUMMARY

Physically vapor-deposited overlay coatings based on the Ni-Cr-Al or Co-Cr-Al (M-Cr-Al) systems are used in the aircraft gas turbine industry because they give better oxidation, hot corrosion, and thermal fatigue protection to turbine airfoils than do aluminide coatings. The oxidation life of a protective coating is controlled by aluminum consumption caused by alumina spalling, erosion, and interdiffusion with the substrate. The relative rates of these processes are determined by coating and substrate composition, service environment, and temperature.

The purposes of this study were (1) to determine the effect of coating and substrate chemistry on the kinetics of interdiffusion and their relation to diffusion-zone constitution and (2) to develop a procedure for analyzing diffusion in multicomponent, multiphase systems. Semi-infinite diffusion couples that had MCrAl sources representative of coatings and sinks representative of nickel- or cobalt-base gas turbine alloys were assembled and annealed at 1000^o, 1095^o, 1150^o, or 1205^o C for as long as 500 hours. The couples were examined by optical microscopy; Knoop microhardness traverses and layer growth measurements were also made.

Parabolic growth constants can be correlated with source aluminum content for a specific sink composition since changes in source aluminum content are more important than changes in chromium content. Sink composition is as important as source composition in determining β recession kinetics in diffusion couples and life in finite coatings. Nickel-base alloys are more stable sources and stronger sinks than cobalt-base alloys. Total and diffusion activation energies were determined from layer growth constants. By introducing the concept of β source strength, which is determined from the appropriate phase diagrams, the Wagner solution for consumption of a second phase in a semi-infinite couple was successfully applied to the analysis of the MCrAl couples. This provided a method (1) for correlating β recession rate constants with couple composition; (2) for determining reliable average total, diffusion, and constitutional activation energies; and (3) for calculating interdiffusion coefficients.

INTRODUCTION

The physically vapor-deposited overlay coatings based on the Ni-Cr-Al (ref. 1) or Co-Cr-Al systems are gaining acceptance in the aircraft gas turbine industry because they give better oxidation, hot corrosion, and thermal fatigue protection to turbine airfoils and have a higher temperature capability than the widely used diffusion aluminide coatings (ref. 2). With higher-use-temperature substrates such as directionally solidified eutectics (ref. 3) and oxide-dispersion-strengthened alloys (ref. 4), the aluminide coatings that successfully protect conventional superalloys offer inadequate diffusional stability. And so the use of overlay coatings is no longer a matter of choice.

The oxidation life of a protective coating in the gas turbine environment is determined by the rate at which aluminum is depleted by alumina spalling and erosion and by interdiffusion with the substrate. The relative rates of these processes are determined by the coating and substrate compositions and by the service environment and temperature. In the case of aluminide coatings, the diffusion reaction between the coating and the substrate has been shown to be far more important than oxidation in determining coating life at 1100° C (ref. 5). It appears that the diffusion reaction is also important in the depletion of overlay coatings, but to a lesser degree. This is based on the following qualitative argument: Typically, overlay coatings are about twice as thick as aluminide coatings (0.013 cm for overlays vs 0.006 cm for aluminides) and have about half the aluminum content on a weight percent basis (12 wt% for overlays vs 25 to 30 wt% for aluminides). If we assume that reduction of the surface aluminum content by 50 percent constitutes aluminum reservoir depletion, the coating's diffusion life t can be computed from the coating thickness h and the interdiffusion coefficient D by

$$t = \frac{h^2}{D} \quad (1)$$

(ref. 6) to a first rough approximation. The depletion criterion seems to be a reasonable one for both coating systems based on the results of Pettit (ref. 7) and Wallwork and Hed (ref. 8). According to Pettit, alloys in the Ni-Al system become spinel formers at about 14-wt% aluminum. Wallwork and Hed found that below about 5-wt% aluminum the NiCrAl and CoCrAl alloys no longer form a continuous protective layer of Al_2O_3 . From equation (1) it is apparent that the double thickness of the overlay coatings could result in a fourfold increase in life over simple aluminide coatings, assuming equal diffusion coefficients. In the Ni-Al system the interdiffusion coefficient is a function of the phase under consideration and its particular chemistry. For example, Janssen (ref. 9) reports that at 1100° C the interdiffusion coefficient for Ni_3Al is $3.6 \times 10^{-10} \text{ cm}^2/\text{sec}$; the interdiffusion coefficient for the saturated terminal nickel solid

solution varies with the source phase from 2.6×10^{-10} cm²/sec with a γ' (Ni₃Al) source to 5.7×10^{-10} cm²/sec with a β (NiAl) source; and the interdiffusion coefficient for 62-at.-%-Ni NiAl is 2.7×10^{-9} cm²/sec. For degradation of an aluminide coating (β) it is reasonable to select the interdiffusion coefficient for β when computing life from equation (1). With an overlay coating the constitution of the diffusion zone is a function of coating and substrate chemistry and can be either γ , γ' , or a mixture of the two. An interdiffusion coefficient of 4.5×10^{-10} cm²/sec is a reasonable average value to use when estimating life for an overlay coating from equation (1). Consequently, one might expect the typical overlay coating to have more than 20 times the life of the typical simple aluminide. A factor of 2 or 3 in life for each coating class may result from variations in diffusivity caused by alloy and coating chemistry.

Alternatively coating life may be improved by controlling the constitution of the diffusion zone through control of coating chemistry and its interaction with alloy chemistry. There is more latitude for accomplishing this with overlay coatings since wide variations in coating chemistry can be readily made.

This study had several purposes. One was to examine the effect of overlay coating chemistry and substrate chemistry on the kinetics of coating depletion by interdiffusion. An associated second purpose was to examine the effect of coating and substrate chemistry on diffusion-zone constitution and mechanical properties. An additional purpose of this study was to develop a procedure for analyzing diffusion in multicomponent, multiphase systems. To accomplish these purposes, semi-infinite diffusion couples were assembled from cast NiCrAl and CoCrAl alloys and annealed at 1000^o, 1095^o, 1150^o, or 1205^o C for as long as 500 hours. The couples were examined by optical microscopy, and Knoop microhardness traverses and layer growth measurements were made. Alloy constitution was established from optical metallography assisted in some instances by the energy dispersive X-ray spectroscopy (EDS) feature of the scanning electron microscope (SEM). Volume fractions of phases present were estimated with an image analyzing computer.

In addition to diffusional stability, other factors such as coefficient of thermal expansion, oxidation resistance, hot corrosion resistance, and mechanical properties are important factors in the selection of an overlay coating chemistry for a particular application. These factors are being examined (refs. 10 and 11).

EXPERIMENTAL PROCEDURES

Alloy Preparation

Nine NiCrAl alloys, nine CoCrAl alloys, and a Ni - 10-wt%Cr alloy were vacuum melted in zirconia crucibles and cast in zirconia shell molds as 5-cm by 10-cm by

0.25-cm slabs. The slabs were ground on both faces to 0.23-cm thickness and then cut into 1.2-cm by 1.2-cm squares. Further details are given by Barrett and Lowell (ref. 11). In addition, stoichiometric NiAl was prepared by electron beam melting in a 2.5-cm by 8-cm copper mold. Nominal alloy chemistries, as determined by atomic absorption spectroscopy, are listed in table I. In figure 1, alloy chemistries of the NiCrAl alloys are plotted on the 1100° C ternary phase diagram. The phase diagram was determined by interpolation from Taylor and Floyd's 1000° and 1150° C phase diagrams (ref. 1). For convenience, the diagram was converted to weight percent. Also shown in figure 1 is the general area in which current and developmental Ni-base turbine blade and vane alloys fall in terms of their Cr and Al contents. Alloys 3S, 4S, 7S, and X are representative of these substrates. Alloys 1C, 2C, 5C, 6C, and 8C are representative of Ni-base overlay coatings, and β is representative of a Ni-base aluminate coating. The "S" and "C" following the alloy numbers designate "substrates" and "coatings," respectively. (The isocyclic oxidation curves presented in fig. 1 are discussed later.) In figure 2, alloy chemistries of the CoCrAl alloys are plotted on an 1100° C ternary diagram (ref. 8). Information for the Co-Cr and Co-Al binaries taken from Hansen (ref. 12) is also shown. Also shown in figure 2 is the general area in which current and developmental high-temperature Co-base alloys fall. Alloy X, which is plotted in figure 2 for illustration, is representative of a Ni-base substrate. Alloy 8'S is representative of a Co-base substrate (primes indicate cobalt-base alloys). The remaining alloys are representative of Co-base overlay coatings.

Isocyclic oxidation performance curves (at 1100° and 1200° C) are plotted on the Ni-Cr-Al and Co-Cr-Al phase diagrams (figs. 1 and 2, respectively). Alloys lying to the left of the curves have poor cyclic oxidation resistance and those to the right have good cyclic oxidation resistance at the indicated temperatures (ref. 11).

Diffusion Couple Fabrication and Heat Treatment

Specimens were prepared for assembly into diffusion couples by wet polishing with 600-grit silicon carbide paper, ultrasonic cleaning, and rinsing with ethanol. All materials were at least 0.18 cm thick by 1.2 cm by 1.2 cm.

The diffusion couples were assembled by stacking the alloys in fixtures made from 304 stainless steel in the order shown in figure 3. All CoCrAl and NiCrAl alloys and β were coupled with alloy X. In addition, four CoCrAl/CoCrAl and four NiCrAl/NiCrAl couples and one CoCrAl/NiCrAl couple were set up. Couples are denoted as follows: source alloy number/sink alloy number, where the source is the alloy richer in aluminum and/or chromium. The stainless-steel fixtures had a square cross section with a slit running the height of one side. Fixture height was adjusted to accommodate all but

half of the thickness of the top coupon in the stack. The bottoms of the fixtures were closed with a piece of 304 stainless-steel sheet that was spot welded to the square-cross-section fixture member. Eight nickel and eight cobalt couples were assembled. Four of the nickel and four of the cobalt couples had intentional markers placed at the weld interfaces. The particles were 2-micrometer $ZrO_2 - 12\text{-wt}\% - Y_2O_3$ particles deposited as a slurry in ethanol.

The couples were hot pressed in their fixtures at 1100°C in vacuum for 1 hour under a stress of about 20 MN/m^2 . Each diffusion-bonded couple was pried from its fixture and then vacuum encapsulated in quartz. The evacuated capsules were backfilled with argon to an absolute pressure of $2 \times 10^4\text{ N/m}^2$ (3 psia) prior to being sealed.

The encapsulated diffusion couples were annealed in horizontal tube furnaces according to the schedule shown in table II. A capsule was slowly inserted into a preheated furnace over a period of about 10 minutes. Temperature was continuously monitored by a strip-chart recording of the signal from an alumina-sheathed Pt/Pt-13%Rh thermocouple located within the alumina furnace tube. Temperature measurements were also made intermittently with a millivolt potentiometer by using the signal from the same thermocouple. Temperature was controlled to within $\pm 8^\circ\text{C}$, with the average temperatures, as determined from the potentiometer readings, deviating no more than 2°C from the temperatures listed in table II. Upon completion of a scheduled anneal, the capsule was slowly withdrawn from the tube furnace over a period of about 10 minutes. About 10 minutes later the capsule was cool enough to open.

Analytical Techniques

The heat-treated diffusion couples were sectioned through the X-X junctions to obtain pieces of convenient size for standard metallographic mounts. The couples were then sectioned along the centerline normal to the weld interfaces and mounted for metallographic preparation with the cut surfaces exposed. The remaining halves of the couples that had been annealed for 500 hours at 1150°C and 1205°C were given an additional 5-hour anneal at 1095°C by using the procedures already outlined. These specimens were also mounted for metallography with the cut surfaces exposed.

The as-cast alloy and diffusion couple metallography specimens were etched with 33 HNO_3 - 33 HCl - 33 glycerol - 1 HF by volume after standard metallographic preparation. Phase identifications were made by optical metallography augmented in some instances by the EDS feature of the SEM. The Ni-Cr-Al (ref. 1) and Co-Al (ref. 12) phase diagrams provided guides for phase identification. The volume fractions of the phases present were estimated on an image analyzing computer.

Microhardness traverses for the couples that had been annealed at 1095°C for 500 hours were made on a microhardness tester to obtain a qualitative indication of the

strength of the alloys and the interdiffusion zones. Microhardness measurements were made with a Knoop indenter driven by a 200-gram load. Filar micrometer measurements of the hardness indentations and the layer growth reactions were made at $\times 100$ or $\times 200$ magnification depending on the distance being measured. Hardness indentation locations were indexed by using the micrometer stage of the hardness tester. The stage micrometer had 0.01-mm divisions.

RESULTS AND DISCUSSION

Alloy Constitution

Photomicrographs of the as-cast Ni-base alloys are presented in figure 4 along with their chemistries and constitutions. The major phase present is always listed first. The constitutions of the as-cast alloys are essentially in agreement with the 1000°C equilibrium diagram of Taylor and Floyd (ref. 1), recognizing that the as-cast alloys are not at equilibrium.

Photomicrographs of the as-cast Co-base alloys are presented in figure 5 along with their chemistries and constitutions. Here, matters are simplified by the absence of the γ' phase in the Co-Cr-Al ternary system. With the exception of alloy 8'S, which is essentially a cobalt solid solution (αCo), the alloys contain β and αCo .

Couples Annealed 500 Hours at 1095°C

Photomicrographs, microhardness profiles, and couple constitutions of the Ni-base couples annealed for 500 hours at 1095°C are presented in figure 6. The positions of the photomicrographs correspond with the abscissas of the microhardness profiles. The faired-in microhardness curves are semiquantitative. In two-phase regions the curves were drawn to approximate the average trend of the composite. From figures 6(a), (b), (e), (f), (k), and (n), it is apparent that the saturated γ phase is quite hard. The $\gamma+\gamma'$ diffusion zones found in couples 1C/X (fig. 6(a)), 2C/X (fig. 6(b)), 6C/X (fig. 6(f)), and 2C/3S (fig. 6(l)) on the source side of the weld are softer than the source. In the first three instances the sink is γ , and the $\gamma+\gamma'$ zone is softer than the saturated γ sink. In couple 2C/3S the γ' phase is formed in the sink, and the $\gamma+\gamma'$ diffusion zone is about as hard as the sink in the vicinity of the weld.

In the β/X couple (fig. 6(j)) the hardness minimum reported by Westbrook for β (ref. 13) is exhibited by the β source in the vicinity of the stoichiometric composition, which is readily locatable from the color change of the NiAl phase from blue to white.

Photomicrographs, microhardness profiles, and the constitutions of couples with Co-base alloy sources annealed for 500 hours at 1095⁰ C are presented in figure 7. The positions of the photomicrographs again correspond with the microhardness profiles, and the faired-in microhardness profiles are again semiquantitative. Solid solutions are designated as either γ (Ni base) or α Co (Co base) depending on whether they were derived from an Ni-base or a Co-base alloy in the as-assembled couples. In almost all cases where the source was α Co+ β and the sink was alloy X (Ni-10Cr, γ) the microhardness profiles display a relative hardness maximum on the alloy X side of the weld and a relative hardness minimum at the weld or on the source side of the weld in the region denuded of β . The only exception was the couple 4'C/X, where a large amount of porosity formed in the vicinity of the weld. Considerable porosity was also formed on the Co-base source side of the weld in the 3'C/X couple.

The data for the volume percent of β in the β -containing NiCrAl and CoCrAl alloys are listed in table I. In figure 8, the average Knoop microhardness for each β -containing alloy is plotted against the volume percent of β . Average microhardness was computed from readings taken in regions unaffected by diffusion after the 500-hour, 1095⁰ C anneal. The range of microhardness values observed for γ and $\gamma+\gamma'$ is indicated at 0-vol% β , and the range for β -NiAl is indicated at 100-vol% β . The hardness data for the β containing NiCrAl alloys is nearly linear with β content and follows the high end of the band defined by the ranges for γ , $\gamma+\gamma'$, and β . The relation of hardness to volume percent of β is also nearly linear for the CoCrAl alloys. Thus, for both systems a rule-of-mixtures relation is being followed.

The constitutions of the Ni-base alloy couples after the 500-hour, 1095⁰ C diffusion anneal are indicated in figure 6 and summarized in table III. Predicted couple constitutions as determined from the ternary phase diagram shown in figure 1 were in agreement with observed constitutions with only a few exceptions. Predictions were based on the phase fields that were crossed by a straight line connecting the source and sink alloys. The persistence of the α phase in alloys 5 and 6 after the 500-hour anneal suggests that some adjustment of the location of the boundary between the $\alpha+\beta+\gamma$ and $\beta+\gamma$ fields is in order. This adjustment will be shown in a revised phase diagram later in the report. An apparent discrepancy between predicted and observed couple constitution was exhibited by the β /X couple. The observed constitution (fig. 6(j)) was β /martensitic $\beta(\beta_M)/\gamma'/\gamma$ although the sequence $\beta/\beta+\gamma'/\gamma'/\gamma+\gamma'/\gamma$ was predicted. The appearance of $\beta+\gamma'$ and an optically visible $\gamma+\gamma'$ structure is sensitive to heat treatment. Rapid cooling of compositions in the β field at 1100⁰ C gives the observed martensitic structure (ref. 14) in preference to $\beta+\gamma'$. At higher nickel content, the absence of an optically visible $\beta+\gamma'$ or $\gamma+\gamma'$ structure is not sufficient evidence for the absence of such a structure. Also, the presence of chromium derived from the alloy X sink tends to suppress γ' formation. Finally, the prediction of couple constitution by assuming a linear diffusion path is at best an approximation, and in reality the path followed can be fairly complex. The

problems of γ' identification and the possible complexity of the diffusion path were also encountered with the 5C/7S couple. Here the observed constitution was $\beta+\gamma+\alpha/\beta+\gamma/\gamma$ although the predicted constitution was $\beta+\gamma+\alpha/\beta+\gamma/\beta+\gamma+\gamma'/\gamma+\gamma'/\gamma$. The straight line connecting alloys 5C and 7S on the ternary phase diagram (fig. 1) crosses the $\beta+\gamma+\gamma'$ and $\gamma+\gamma'$ fields within 0.5 wt% of the composition at which the γ' phase can no longer exist. This is within the expected error in the construction of the phase diagram. Finally, the observed constitution for the 8C/4S couple was $\beta+\gamma/\gamma/\gamma+\gamma'/\gamma$ although the predicted constitution was $\beta+\gamma/\gamma$. This discrepancy suggests that a complex diffusion path was followed and that predictions based on a linear path can serve only as a guide. In any case, the small volume fraction of γ' found on the alloy 4S side of the weld will have a small effect on the kinetics of interdiffusion.

Cobalt-base couple constitutions after the 500-hour, 1095^o C anneal are indicated in figure 7 and summarized in table III. In those cases where alloy X (Ni-10Cr, γ) was the sink, the couple constitutions are precisely what one might expect for a Co-10Cr sink. No γ' phase is evident on the sink side of the weld, and the constitutions were $\beta+\alpha\text{Co}/\alpha\text{Co}/\gamma$ in those couples having β in the source alloy. In those couples with a Co-base source and sink the constitutions are in agreement with the ternary phase diagram shown in figure 2. The 9C/9'C couple shown in figure 7(n) is noteworthy. Here the Co-base alloy was $\beta+\alpha\text{Co}$ and the Ni-base alloy was $\gamma+\gamma'$. The couple constitution after the 500-hour, 1095^o C anneal was $\beta+\alpha\text{Co}/\alpha\text{Co}/\beta+\gamma/\gamma'/\gamma+\gamma'$. This illustrates the stronger β -forming tendency of Ni-base alloys as compared with Co-base alloys.

Layer Growth Kinetics

In this section, layer growth data for couples annealed at 1095^o and 1205^o C for as long as 500 hours are discussed. From layer growth in the semi-infinite couples some inferences about finite coating life are drawn. In addition, the locations of markers relative to the welds are discussed. Finally, activation energies for layer growth are treated.

Two activation energies for layer growth can be reported in this kind of study. The first is called the diffusion activation energy Q_D and corresponds with the conventional diffusion activation energies reported in the literature for diffusion in simple single-phase systems ($D = D_0 e^{-Q_D/RT}$). The diffusion activation energy, as defined by this author, completely discounts the effects of temperature on the constitution of the ternary systems. The second activation energy is called the total activation energy Q_T which is equal to the sum of the diffusion activation energy plus an activation-energy-like quantity that accounts for the effect of temperature on the constitution of the ternary system. This latter quantity is called the constitutional effect or the constitutional

activation energy Q_C . The total activation energy was determined from layer growth in the couples annealed for 500 hours. The diffusion activation energy was to be computed from layer growth in the 500-hour, 1095° C couples and the couples aged for 5 hours at 1095° C after their 500-hour 1150° and 1205° C anneals. This 5-hour anneal was intended to remove the constitutional effect by bringing all couples to a 1095° C base in terms of constitution. However, the fine precipitates generated in the diffusion zone by the aging treatments could not be identified with certainty in the majority of the Ni-base couples. Therefore, at this point, only total activation energies are reported for these couples. With the Co-base couples the intended purpose of the aging treatments was successfully achieved. For these couples, total and diffusion activation energy and the constitutional effect are reported. In many cases a linear Arrhenius relation was not obtained over the entire temperature range. In these instances, activation energy was computed by using data from only the three higher temperatures.

Nickel-base couples. - Layer growth data for Ni-base couples annealed at 1095° or 1205° C for as long as 500 hours are plotted in figure 9 as thickness against square root of time. Parabolic growth constants k for layer growth are listed in table III.

Data for martensitic β (really martensitic β and what appears to be submartensitic β) and γ' growth in the β/X couple are plotted in figure 9(a). The growth of the γ' layer is relatively insensitive to temperature as compared with the growth of the martensitic β layer. The growth of the martensitic β zone is quite rapid even at 1095° C when one considers that aluminide coatings are generally used at about 75- μm thickness, as deposited, and grow to about 150 μm in service as a result of interdiffusion with the substrate at this temperature. The appearance of the martensitic β structure in an aluminide coating can be considered indicative of exhaustion of a coating's useful life since oxidation resistance falls off rapidly when NiAl is depleted below 40-at.% Al (refs. 5 and 14). In the semi-infinite couples a 150- μm -thick martensitic β (plus submartensitic β) layer was formed in about 150 hours at 1095° C and in 10 hours at 1205° C. These times can be considered indicative of the oxidation life of a conventional aluminide coating on a simple Ni-10Cr substrate.

Markers in the β/X couples were located just in the β phase close to the β/γ' interface. The weld location in these couples could not be precisely established, but it appeared to be located between the β_M and γ' interfaces. This indicates that the net flux of Ni and Cr into β exceeds that of aluminum out of β , as might be expected from the results reported by Janssen (ref. 9) and others. Earlier, it was noted that the $\gamma+\gamma'$ and $\beta+\gamma'$ structures were not visually detected in the 1095° C, 500-hour couple. The $\beta+\gamma'$ structure was apparent only in the couples annealed at 1205° C. The aging treatment of the 500-hour, 1150° and 1205° C couples at 1095° C for 5 hours gave obvious $\beta+\gamma'$ and $\gamma+\gamma'$ structures but had no significant effect on the growth data, as can be seen from figure 9(a).

The total activation energy for growth of substoichiometric $\beta+\beta_M+\gamma'$ submartensitic $\beta+\gamma'$ was 261 kJ/mole (62.5 kcal/mole). At 1000° C the β_M zone was not observed. The total activation energy for growth of $\beta_M+\gamma'$ at the three higher temperatures was 426 kJ/mole (102 kcal/mole). The total activation energy for growth of γ' was 186 kJ/mole (44.5 kcal/mole).

Data for the recession of the β phase in Ni-base couples are plotted in figures 9(b) to (d). The source alloy chemistries can be considered representative of contemporary overlay coating compositions; and sink alloys X, 3S, 4S, and 7S can be considered representative of a range of substrate compositions. The effect of chromium content at constant aluminum content can be seen from comparison of couples 6C/X and 1C/X, (figs. 9(b) and (c), respectively). The parabolic rate constant for β recession k at 1095° C in 6C/X is 4.4×10^{-11} cm²/sec, while in 1C/X it is 1.1×10^{-10} cm²/sec. The 4.6-wt% decrease in chromium content in going from 6C/X to 1C/X results in a 2.5-fold increase in the β recession rate (or a rate of increase of about 54 percent per wt% decrease in Cr content). The effect of changes in aluminum content on k was computed by assuming that the effect of chromium content was 54 percent in all cases. The average effect of a 1 percent decrease in aluminum content was a 240 percent increase in k . Based on the limited number of alloys studied, the average effect was 150 percent in going from $\beta+\gamma+\gamma'$ to $\beta+\gamma$ alloys, 400 percent in going from $\beta+\gamma+\gamma'$ to $\beta+\alpha+\gamma$ alloys, 210 percent within the $\beta+\gamma$ field, 90 to 480 percent (260 percent average) in going from $\beta+\gamma$ to $\beta+\gamma+\alpha$ alloys, and 60 percent within the $\beta+\alpha+\gamma$ field. Thus, changes in aluminum content are at least as important as, and in some instances about 10 times more important than, changes in chromium content in terms of composition effects on β recession rate.

If one considers only couples with an alloy X sink, a reasonable correlation between the parabolic rate constant for β recession (table III) and either the aluminum content of the source or the volume percent of β in the source is obtained as suggested by the generally greater importance of changes in aluminum content as compared with changes in chromium content. This correlation is reasonable in view of the fact that the driving potential for the reaction is defined by the $\beta+\gamma/\gamma$ boundary, which is at approximately constant aluminum content (fig. 1). The problem with this type of correlation is that it cannot be readily generalized to include variation of the sink composition. The great importance of sink composition in these semi-infinite diffusion couples and of substrate composition in the case of finite coatings can be seen by comparing recession rates (in cm²/sec) at 1095° C in the following sets of couples: 5C/X ($k = 2.0 \times 10^{-11}$) with 5C/7S ($k = 3.6 \times 10^{-13}$), figure 9(b); 2C/X ($k = 3.6 \times 10^{-10}$) with 2C/3S ($k = 1.6 \times 10^{-10}$), figures 9(c) and (d), respectively; 8C/X ($k = 6.4 \times 10^{-10}$) with 8C/4S ($k = 1.4 \times 10^{-10}$), figures 9(c) and (d), respectively. With source 5C the driving force in terms of weight percent of aluminum decreased by 18 percent in going from the alloy X sink to the alloy

7S sink while the rate constant decreased by nearly two orders of magnitude. With source 2C the driving potential decreased by 51 percent in going from the alloy X sink to the alloy 3S sink while the rate constant decreased by 50 percent. With source 8C the driving potential decreased by 63 percent in going from the alloy X sink to the alloy 4S sink while the rate constant decreased by 78 percent. The sink effect is thus clearly not described by a simple linear relation. A workable method for correlating kinetics with source and sink composition is discussed later.

In all couples where β recession was the most significant reaction (figs. 9(b) to (d)) the weld interface and marker interface were nearly coincident. Microstructurally, the aging treatment produced γ envelopes around particles of β in the essentially $\beta+\gamma$ region and fine precipitates in the region denuded of β both on the source side of the weld and on the sink side of the weld in the aluminum-enriched region. The identity of these precipitates could not be established. In addition, fine precipitates of presumably αCr were developed within β particles, and fine plates were precipitated in γ coexisting with β in alloys 1C, 2C, 5C, and 6C but not in alloy 8C.

Total activation energies for β recession are listed in table III. Total activation energies ranged from 288 to 426 kJ/mole (68.9 to 102 kcal/mole) with a mean value of 328 kJ/mole (78.4 kcal/mole). The highest total activation energies were observed for couples whose source alloys had lower β contents. For example, total activation energies of 360 and 426 kJ/mole (86.2 and 102 kcal/mole) were observed for the 8C/X and 8C/4S couples, respectively. Because the identity of the fine precipitates generated in the diffusion zone by the aging treatments could not be established, the diffusion activation energy could not be determined for the Ni-base couples.

The 5C/7S couple, which was not included in the preceding discussion of total activation energy, displayed noteworthy behavior. For this couple, two reactions occurred: conversion of $\beta+\alpha+\gamma$ to $\beta+\gamma$ and recession of β . The same situation is true for the 6C/X and 5C/X couples, but only the first reaction occurs in the 6C/1C couples. Data for couples showing the $\beta+\alpha+\gamma$ to $\beta+\gamma$ reaction at 1095⁰ C are plotted in figure 9(e) in terms of the total reaction. Comparison with figure 9(b) shows that the total reaction is about an order of magnitude more rapid than β recession. At higher temperatures the semi-infinite boundary condition for the total reaction broke down in these couples. The activation energy determined for β recession in the 5C/7S couple was 777 kJ/mole (186 kcal/mole). The low recession rate constant and high activation energy observed for the 5C/7S couple suggest that increased aluminum content of the alloy 7S sink vis-a-vis alloy X has brought the couple to the point where at infinite time the equilibrium composition is just outside the $\beta+\gamma$ phase field. A further increase in the aluminum content of the source or sink might result in the advance of the β phase rather than its recession as was the case in the β /X couple. In going from one case to the other, k will approach zero and Q will approach infinity, for a system whose constitution is not a function of temperature. In the Ni-Cr-Al system the strong effect of temperature on

constitution influences the activation energy determined from phase recession. This is particularly true of the 5C/7S couple, whose average composition is close to the phase boundary. More will be said about the question of constitutional and diffusion activation energies later.

The recession of γ' in the 9C/X couple at 1095° and 1205° C is plotted in figure 9(f). Since alloy 9C is close to the $\gamma+\gamma'/\gamma$ phase boundary, the effect of temperature on the constitution of the system strongly influenced the activation energy determination. A total activation energy of 497 kJ/mole (119 kcal/mole) was determined for this couple.

Cobalt-base couples. - Data for recession of the β phase in couples with a Co-base source are plotted in figure 10. In figures 10(a) to (c) the sink is alloy X. The effect of changing from a Co-base source to a Ni-base source without a significant change in source chromium or aluminum content can be seen by comparing the 5'C/X and 6C/X couples. The Co-base source exhibits β recession rate constants of $6.7 \times 10^{-11} \text{ cm}^2/\text{sec}$ at 1095° C and $6.1 \times 10^{-10} \text{ cm}^2/\text{sec}$ at 1205° C. The Ni-base source exhibits β recession rate constants of $4.4 \times 10^{-11} \text{ cm}^2/\text{sec}$ at 1095° C and $7.0 \times 10^{-10} \text{ cm}^2/\text{sec}$ at 1205° C. The Ni-base source is therefore apparently more stable at 1095° C than the Co-base source but loses this advantage at 1205° C. This change in relative stability may be partly or entirely due to differing effects of temperature on the constitution of the ternary systems. This subject is treated later.

The effect of changes in chromium content on β recession can be seen by comparing couples 6'C/X and 9'C/X. In 6'C/X the difference in chromium content between source and sink is 0.4 wt%, and the β recession rate constant at 1095° C is $1.5 \times 10^{-10} \text{ cm}^2/\text{sec}$; in 9'C/X the difference is 12.1 wt%, and the rate constant is $1.0 \times 10^{-10} \text{ cm}^2/\text{sec}$. The 11.7-wt% decrease in chromium content in going from 9'C/X to 6'C/X results in a 1.5-fold increase in β recession rate (or a rate of increase of about 13 percent per wt% decrease in Cr content). Thus, the effect of chromium content on β recession in Co-base source couples is about one-fourth the magnitude of the effect in Ni-base source couples.

Because of the small effect of chromium content in couples with a Co-base source, couples 4'C/X and 5'C/X can be compared to assess the effect of aluminum content on β recession rate. In couple 4'C/X the difference in aluminum content between source and sink is 5.8 wt%, and the β recession rate constant is $2.6 \times 10^{-10} \text{ cm}^2/\text{sec}$ at 1095° C; in 5'C/X the difference is 12.5 wt%, and the rate constant is $6.7 \times 10^{-11} \text{ cm}^2/\text{sec}$. The 6.7-wt% decrease in aluminum content in going from 5'C/X to 4'C/X results in a 3.9-fold increase in β recession rate (or a rate of increase of about 58 percent per wt% decrease in Al content). The computed sensitivities of k to changes in chromium and aluminum content are valid throughout the $\beta+\alpha\text{Co}$ two-phase field. The effect of changes in aluminum content on β recession is weaker than was observed with Ni-base couples. The relative importance of changes in aluminum content as compared with

changes in chromium content is about the same whether the source alloy is cobalt base or nickel base.

As was the case with Ni-base couples, β recession rate constants for Co-base source/alloy X sink couples (table III) can be correlated with either source aluminum content or volume percent of β . The data presented in figures 10(a) to (c) are arranged with the couples with the largest driving potentials and lowest rates in part (a) (2'C/X, 7'C/X, 5'C/X), those with intermediate potentials and rates in part (b) (6'C/X, 1'C/X, 9'C/X), and those with the smallest potentials and highest rates in part (c) (3'C/X and 4'C/X). At 1205^o C the β phase was not stable in alloy 3'C.

In all Co-base source couples the marker and weld interfaces were coincident. The aging treatment was much more straightforward with the Co-base alloys since the only likely phase precipitating was β , although in some cases σ cannot be ruled out. In all cases the 5-hour, 1095^o C aging of couples annealed for 500 hours at either 1150^o or 1205^o C produced acicular precipitates in α Co and β particles in the $\beta+\alpha$ Co region and in part of the α Co depleted zone. In the 3'C/X couple where β was dissolved at 1205^o C, aging produced acicular precipitates. The β recession measurements for the aged 500-hour, 1205^o C couples are plotted in figures 10(a) to (c). Since these precipitates are presumably β , the total and diffusion activation energies are reported in table III. The total activation energy for β recession in Co-base source/alloy X sink couples ranges from 334 to 431 kJ/mole (79.8 to 103 kcal/mole) with a mean value of 376 kJ/mole (90.0 kcal/mole). Note that the highest values (372 to 431 kJ/mole (89 to 103 kcal/mole)) were observed for the five compositions closest to the $\beta+\alpha$ Co/ α Co phase boundary (fig. 1). These couples display the greatest sensitivity to constitutional effects, as was the case with the Ni-base couples. The diffusion activation energies determined from the aged couples and the 1095^o C couple ranged from 255 to 367 kJ/mole (60.9 to 87.7 kcal/mole), with mean value of 298 kJ/mole (71.2 kcal/mole). The difference between the total and diffusion activation energies ranged from 46.8 to 107 kJ/mole (11.2 to 25.7 kcal/mole), with a mean value of 78.6 kJ/mole (18.8 kcal/mole). The largest values of the difference, which represents the effect of constitution, were observed for those couples closest to the $\beta+\alpha$ Co/ α Co phase boundary.

The kinetics of β recession in a couple with a Co-base source and sink (4'C/8'S) are plotted in figure 10(d). Since the source and sink are relatively close to the $\beta+\alpha$ Co/ α Co phase boundary, the aging treatment has a large effect on measured β recession, as shown. The total activation energy for β recession in the 4'C/8'S couple was 598 kJ/mole (143 kcal/mole) and the diffusion activation energy was 184 kJ/mole (44.0 kcal/mole).

The kinetics of β recession in a couple with a Co-base source and $\gamma+\gamma'$ Ni-base sink are shown in figure 10(e). In this couple (9'C/9C, fig. 7(n)) β is formed on the sink side of the weld. The growth of $\beta+\gamma$ and γ' in the sink is also plotted in figure 10(e). In this

couple, aluminum is apparently diffusing as a result of the initial concentration gradients of chromium, nickel, and cobalt since there was no initial aluminum concentration difference across the weld. The rate of β recession in alloy 9'C is comparable to rates observed in Co-base source/alloy X sink couples with the smallest aluminum concentration differences. The total and diffusion activation energies for β recession in the source were 375 and 314 kJ/mole (89.8 and 75.1 kcal/mole), respectively. The total activation energy for $(\beta+\gamma)+\gamma'$ growth in the sink was 387 kJ/mole (92.5 kcal/mole).

Finite coating life. - A first-order estimate of finite coating life based solely on diffusional degradation can be made from the recession data obtained from the semi-infinite couples by assuming that the time for β to recede a distance equal to the finite coating thickness in the semi-infinite couple approximates finite coating life. This life estimate can be qualitatively tempered to account for the cyclic oxidation performance of alloys at the $\gamma/\beta+\gamma$ phase boundaries in the Ni-Cr-Al system (fig. 1) or the $\alpha\text{Co}/\beta+\alpha\text{Co}$ phase boundary in the Co-Cr-Al system (fig. 2). Finite overlay MCrAlY coatings are generally applied in 0.013-cm (~ 5 -mil) thicknesses. Life based on diffusional degradation is then given by

$$t \approx \frac{h^2}{k} = \frac{(0.013)^2}{k} \text{ sec} = \frac{4.7 \times 10^{-8}}{k} \text{ hr} \quad (2)$$

Results are listed in table IV. Qualitative adjustments based on cyclic oxidation performance are indicated by $>$ or $<$. In general, lives based on diffusional degradation of the β -containing coatings to the terminal solid solution are conservative for the Ni-base alloys and somewhat unconservative for the Co-base alloys at 1095^o C, based on the relative positions of the phase boundaries and the isocyclic oxidation curves in figures 1 and 2. At 1205^o C the diffusion lives are somewhat conservative for the Ni-base alloys and unconservative for the Co-base alloys.

Comparing the predicted lives of couples 8C/4S with 8C/X, 4'C/8'S with 4'C/X, 5C/7S with 5C/X, and 2C/3S with 2C/X discloses the great importance of substrate composition in determining coating life. The effect can be as large as the effect of coating composition on coating life. Comparing the lives of couples 6C/X with 5'C/X, where essentially the only difference in chemistry is the base metal of the source, reveals that Ni-base coatings are superior to Co-base coatings on a Ni-base alloy. The effect of coating composition on coating life follows directly from the effects of composition on the β recession rate constant discussed earlier. Increases in chromium content are beneficial to both Co-base and Ni-base coatings with life increasing about 13 percent per wt% increase in chromium content with the Co-base alloys and 54 percent per wt% increase in chromium content with the Ni-base alloys. However, the effect is not as important as changes in aluminum content. Life increases by about 58 percent per

wt% increase in aluminum content in Co-base coatings and by a least 60 percent per wt% increase in aluminum content in Ni-base coatings. In the Ni-base coatings the strength of the effect is a function of the phase field and the location within the phase field.

Analysis of Layer Growth Data

A solution to the solid-state diffusion problem illustrated in figure 11 was developed by Wagner (ref. 15) for the case where there is assumed to be no diffusion in phases I and II. Under this assumption the problem is the same as the diffusion problem posed by many of the semi-infinite couples in this study if the γ' and α phases are neglected. Wagner's solution is

$$\xi^2 = 4g^2 D_{II} t \quad (3)$$

where the dimensionless parameter g is defined by

$$Z = \frac{C_{II,0} - C_{II,I}}{C_{II,I} - C_0} = \sqrt{\pi} g \exp(g^2)(1 + \operatorname{erf} g) \quad (4)$$

D_{II} is the diffusion coefficient in phase II; t is the time; $C_{II,0}$ and C_0 are the initial compositions of the sink and source, respectively; and $C_{II,I}$ is the composition of phase II at the interface as illustrated in figure 11. The term $4g^2 D_{II}$ is the same as the β recession rate constant k used earlier in this report. The diffusion coefficient can be represented by the Arrhenius relation

$$D_{II} = D_0 e^{-Q_D/RT} \quad (5)$$

where D_0 is a constant, Q_D is the diffusion activation energy, R is 8.31 J/mole-K (1.987 cal/mole-K), and T is the absolute temperature in Kelvin.

The dimensionless parameter g is a complex function of composition (eq. (4)), as illustrated in the schematic phase diagram (fig. 12). The location of the boundary between phase II and phases I and II that partially defines $C_{II,I}$ can be represented by an Arrhenius relation. The location of $C_{II,I}$ on the boundary is determined from diffusion along a minimum-free-energy path, and this is a complex function of diffusion coefficients and partial molar free energies. These too can be represented by Arrhenius relations.

Wagner's solution cannot be directly applied to the diffusion problems of this study

since we do not know $C_{II,I}$. However, $C_{II,I}$ can be estimated from the straight line connecting the terminal compositions in figure 12. This is a reasonable approximation since the location of the phase boundary is a weak function of chromium content in the Ni-Cr-Al and Co-Cr-Al systems. The quantity $a/(a + b)$ illustrated in figure 12 is called the β source strength B . The relation between β source strength and Z is

$$B = \frac{1}{1 + Z} \quad (6)$$

The dimensionless parameter g is related to the β source strength as illustrated by the calculated solid curve in figure 13. For the range of B values of interest ($0.01 < B < 0.8$)

$$\ln g^2 = -aB + b \quad (7)$$

or

$$g^2 = e^{-aB+b} \quad (8)$$

fits the curve to within a factor of 2. The rate constant can then be written for temperature T_1 as

$$k_1 = 4e^{-aB_1+b} D_0 e^{-Q_D/RT_1} \quad (9)$$

and for T_2

$$k_2 = 4e^{-aB_2+b} D_0 e^{-Q_D/RT_2} \quad (10)$$

Then the ratio of β recession rate constants for T_1 and T_2 is given by

$$\frac{k_1}{k_2} = e^{a(B_2-B_1) - (Q_D/R) [(1/T_2)-(1/T_1)]} \quad (11)$$

Let β source strength be represented by an Arrhenius relation

$$B = B_0 e^{-Q_C/RT} \quad (12)$$

and

$$T_2 = T_1 + dT \quad (13)$$

Then

$$\frac{k_1}{k_2} = \exp \left\{ aB_0 \left[e^{-Q_C/R(T_1+dT)} - e^{-Q_C/RT_1} \right] \right\} \exp \left[\frac{Q_D}{R} \left(\frac{1}{T_1 + dT} - \frac{1}{T_1} \right) \right] \quad (14)$$

By expansion in series and combination of higher-order terms, a simplification of the exponent of the first exponential is obtained

$$aB_0 \left[e^{-Q_C/R(T_1+dT)} - e^{-Q_C/RT_1} \right] = aB_0 \frac{Q_C}{RT_1^2} e^{-Q_C/RT_1} \quad (15)$$

Therefore,

$$\frac{k_1}{k_2} = e^{aB_1(Q_C/R)(dT/T_1^2)} e^{(Q_D/R)(dT/T_1^2)} \quad (16)$$

Letting

$$aB_1 Q_C = Q'_C \quad (17)$$

gives

$$\frac{k_1}{k_2} = e^{-(Q'_C/R)(dT/T_1^2)} e^{-(Q_D/R)(dT/T_1^2)} = e^{-(Q_T/R)(dT/T_1^2)} \quad (18)$$

Equation (18) shows that the total activation energy for β recession Q_T is equal to the sum of the diffusion activation energy Q_D and an activation-energy-like term Q'_C that accounts for the effect of temperature on the constitution of the ternary system.

From equation (9) it is apparent that a plot of $\log k$ against B should be linear for a group of similar diffusion couples run at the same temperature. If for T_1 we plot the $\log k_1$ values against their respective B_1 values and for T_2 we plot the $\log k_2$ values against their respective B_2 values, we should get two nearly parallel straight

lines. From equation (11) it is apparent that, from the ratio of k_1/k_2 at constant B , we can determine Q_D for the family of diffusion couples.

The data for the T_2 couples after aging at T_1 for a short time ($k_{2, \text{aged}}$) can properly be plotted against B_1 values. Since the purpose of the aging treatment was to remove the effect of temperature on phase constitution, the lines for $\log(k_{2, \text{aged}})$ against B_1 and $\log k_2$ against B_2 should be colinear.

Finally, the average activation energy determined from the k_1/k_2 ratios of the individual couples gives Q_T as already discussed. These data can be put on the same plot as $\log k_1$ against B_1 , $\log k_2$ against B_2 , and $\log(k_{2, \text{aged}})$ against B_1 by arbitrarily plotting $\log k_2$ against B_1 or $\log k_1$ against B_2 . Since $\log(k_{2, \text{aged}})$ against B_1 will be plotted, the former scheme will be used. Then the ratio of k_1/k_2 at fixed B_1 gives Q_T at B_1 .

To construct the plots just described, B must be determined at 1095° and 1205° C for each diffusion couple. In figure 14 the estimated 1100° C ternary Ni-Cr-Al phase diagram of figure 1 is repeated. An estimated partial 1200° C phase diagram is also plotted. The method of determining B for couple 5C/X at 1100° C is illustrated in figure 14. Values of B and k for the Ni-base couples are listed at the top of table V.

The plot of $\log k$ against B for the Ni-base couples is presented in figure 15. With the exception of couple 5C/7S, which did not obey the semi-infinite boundary condition because the reaction proceeded by a dual mechanism, the relation between $\log k$ and B is linear over a wide range of both variables at 1095° and 1205° C. The fitted linear regression lines are nearly parallel. Parallel lines would indicate that the total, diffusion, and constitutional activation energies are constant. The most reliable B values are determined for large B . Consequently, the activation energies were computed at $B = 0.5$, as shown in figure 15. These activation energies are called average activation energies to distinguish them from the mean activation energies determined earlier from layer growth measurements on individual couples. At $B = 0.5$, average total, diffusion, and constitutional activation energies of 372, 268, and 105 kJ/mole (89, 64, and 25 kcal/mole), respectively, were computed. The average total activation energy is in excellent agreement with the 289-kJ/mole (69.2-kcal/mole) activation energy reported for nickel self-diffusion (ref. 16, average of most reliable values) and with the 268-kJ/mole (64.0-kcal/mole) activation energy reported for aluminum diffusion in a nickel solid solution (ref. 17). More recently, Janssen (ref. 9) reported activation energies of 272 kJ/mole (65 kcal/mole) for volume diffusion in an aluminum-saturated, nickel solid solution and 268 kJ/mole (64 kcal/mole) for Ni_3Al . Hancock (ref. 18) reported a value of 303 kJ/mole (72.4 kcal/mole) for Ni-tracer diffusion in Ni_3Al .

Interdiffusion coefficients were computed from the Wagner solution (eq. (3)) by using the relation between B and g illustrated in figure 13. Results for the Ni-base

couples are listed in the top half of table V. At 1095^o C the average diffusion coefficient computed from the individual couples was 8.3×10^{-11} cm²/sec. At 1205^o C the average diffusion coefficient was 3.8×10^{-10} cm²/sec. The large amount of scatter in the computed D values is due to a combination of errors in the determination of B from the estimated phase diagrams and the variable adequacy of the assumptions made in using the Wagner solution. The average diffusion coefficients computed are in reasonable agreement with data reported in the literature. Swalin, et al. (ref. 17) report diffusion coefficients of 1.1×10^{-10} cm²/sec for aluminum in γ at 1095^o C and 6.4×10^{-10} cm²/sec at 1205^o C. By using the average of the most reliable data compiled by Askill (ref. 16), nickel self-diffusion coefficients of 2.0×10^{-11} cm²/sec at 1095^o C and 1.4×10^{-10} cm²/sec at 1205^o C were computed. The results obtained in this study are very close to the average of the nickel self-diffusion coefficient and the diffusion coefficient for aluminum in nickel: 6.5×10^{-11} cm²/sec at 1095^o C and 3.9×10^{-10} cm²/sec at 1205^o C.

To correlate and analyze the β recession data for the Co-base source/alloy X sink couples, an accurate ternary phase diagram was required. An 1100^o C diagram was constructed by using the data from Hansen (ref. 12) shown in figure 2 and the volume-percent- β data listed in table I. The latter information permitted the locations of the α Co/ β + α Co and β + α Co/ β boundaries to be estimated. The β + σ + α Co boundary was positioned somewhat arbitrarily. The estimated 1100^o C Co-Cr-Al phase diagram is shown in figure 16. The 1200^o C α Co/ β + α Co boundary is considered to be more accurate than the 1100^o C boundary since it was well defined by data from the Co-Al binary (ref. 12) and the fact that β was present in alloy 4'C at 1200^o C but was absent in alloy 3'C.

The procedure for determining β source strength B is illustrated for the 1'C/X couple at 1100^o C in figure 16. The Ni-10Cr sink data point was plotted at 10Cr such that its average distance from the α Co/ β + α Co boundary was the same as its average distance from the γ / β + γ or γ' / β + γ + γ' boundary in the Ni-Cr-Al system. This reflects the fact that, for Ni- and Co-base alloys having the same chromium and aluminum content, the Ni-base alloy is the stronger sink for aluminum.

Values of β source strength and β recession rate constant at 1095^o and 1205^o C for the Co-base source/alloy X sink couples are listed in the lower half of table V. The β recession rate constants for the aged couples $k_{2, \text{aged}}$ were calculated from the data points for each aged couple. These data are plotted in figures 10(a) to (c). The plots of β recession rate constant against β source strength are shown in figure 17. The fitted linear regression lines are not perfectly parallel, which indicates some variation in activation energy with B. Since the most reliable B values are determined when B is large, average activation energies were computed for B = 0.5, as illustrated in figure 17. The average total, diffusion, and constitutional activation energies are 343, 286, and 56.8 kJ/mole (82.0, 68.4, and 13.6 kcal/mole), respectively. The average activation energies fall within the respective activation energy ranges determined earlier

for the individual couples. The average diffusion activation energy falls between the most reliable self-diffusion activation energies reported by Askill (ref. 16) for cobalt and nickel: 283 and 289 kJ/mole (67.7 and 69.2 kcal/mole), respectively.

The average total activation energy for the Ni-base couples is 29 kJ/mole (7 kcal/mole) higher than that for the Co-base source/alloy X sink couples, but the average diffusion activation energy is about 17 kJ/mole (4 kcal/mole) lower. The net result is a constitutional activation energy about 46 kJ/mole (11 kcal/mole) higher for the Ni-base source. The effect of temperature on the constitution of the β -containing multiphase fields in the Ni-Cr-Al system is stronger than in the Co-Cr-Al system in the 1100^o to 1200^o C temperature range.

Diffusion coefficients computed from the Wagner solution are listed in the lower half of table V. They fall within a very narrow band at both 1095^o and 1205^o C. The diffusion coefficients are representative of a terminal solid solution that has small chromium and aluminum concentration gradients relative to the large gradients for cobalt and nickel since the diffusion zone is Ni-rich at the sink and Co-rich in the vicinity of the source. These diffusion coefficients can be applied in the analysis of a CoCrAlY coating on a simple Ni-base substrate or to a NiCrAlY coating on a simple Co-base substrate. The average diffusion coefficients for the Co-base source/alloy X sink couples are somewhat larger than average diffusion coefficients for the Ni-base couples.

Finally, the Co-base source/Co-base sink couple 4'C/8'S was analyzed, as shown at the bottom of table V. The diffusion coefficient is considered reliable at 1095^o C but open to question at 1205^o C because of the uncertainty associated with measuring small B values.

SUMMARY OF RESULTS

Semi-infinite diffusion couples having NiCrAl or CoCrAl sources representative of overlay or aluminide coatings and sinks representative of Ni- or Co-base turbine blade or vane alloys were assembled and annealed at 1000^o, 1095^o, 1150^o, or 1205^o C for as long as 500 hours. The couples were examined by optical microscopy; Knoop microhardness traverses and layer growth measurements were also made. The following results, classified according to purpose, were obtained:

1. Purpose - To determine the effect of coating and substrate chemistry on diffusion kinetics and diffusion-zone constitution:
 - a. Layer growth and β recession followed parabolic growth equations.
 - b. For a specific sink composition the β recession rate constant can be correlated with the source aluminum content or the source volume percent of β in couples with either Co-base or Ni-base sources.

c. Sink composition can be as important as source composition in determining β recession kinetics in semi-infinite couples. This would also be true of substrate composition in dealing with diffusional degradation of a finite coating.

d. Nickel-base alloys have a greater affinity for aluminum and a stronger tendency to form β than Co-base alloys. This makes a Co-base source less stable than a Ni-base source of the same chemistry on a Ni-base alloy.

e. In Ni-base couples with a β -containing source, a 1-wt% decrease in chromium content increases the β recession rate by 54 percent. The average effect of a 1-wt% decrease in aluminum content is a 240-percent increase in the β recession rate. The magnitude of the aluminum effect is related to the specific source composition and constitution.

f. In Co-base source/alloy X (Ni-10Cr) sink couples, a 1-wt% decrease in chromium content increased the β recession rate by 13 percent. A 1-wt% decrease in aluminum content increased the β recession rate by 58 percent.

g. The activation energies determined from β recession or layer growth rate constants are the sum of the diffusion activation energy plus an activation-energy-like term that reflects the effect of temperature on the constitution of the system.

h. Diffusion activation energies can be determined from layer growth measurements by eliminating the effect of temperature on constitution by aging the high-temperature, long-time couples for a short time at a common low temperature and remeasuring layer growth. The aging method was applied successfully to the Co-base alloy source couples but was not successful with the Ni-base alloy source couples because phase identification of the fine precipitates generated could not be positively made.

i. For the Ni-base couples, the mean total activation energy determined from β recession kinetics of the individual couples was 328 kJ/mole (78.4 kcal/mole). Total activation energy increased as the β content of the source alloy decreased.

j. For the Co-base source/alloy X sink couples, the mean total activation energy was 376 kJ/mole (90 kcal/mole) and the mean diffusion activation energy was 298 kJ/mole (71.2 kcal/mole), as determined from β recession rate constants and averaged over all couples in the group. The mean constitutional effect, which is the difference between the activation energies, was 78.6 kJ/mole (18.8 kcal/mole). The total activation energy and the constitutional effect increased as the β content of the couples decreased.

k. Couple constitutions in the Ni-Cr-Al system were predicted reasonably well from the phase fields that were crossed on the ternary phase diagram by the straight line connecting the couple terminal compositions.

2. Purpose - To develop a procedure for analyzing diffusion in multiphase, multi-component systems:

a. By introducing the concept of β source strength that can be readily determined from the appropriate phase diagrams, the Wagner solution for consumption of a second phase in a semi-infinite couple was successfully applied to the analysis of β recession in the multiphase, multicomponent NiCrAl and CoCrAl diffusion couples studied. Applying the Wagner solution by using the β source strength concept provided a method for correlating β recession rate constants with couple compositions; a method for determining reliable average total and diffusion activation energies and the magnitude of the constitutional effect; and, finally, a method for calculating diffusion coefficients.

b. The source strength concept should be useful in analogous diffusion problems encountered in other systems.

c. The β recession rate constant k was related to the β source strength by

$$k = 4D e^{-aB+b}$$

where a and b are constants and D is the interdiffusion coefficient of the diffusion zone.

d. For the Ni-base couples, the average total and diffusion activation energies and the average constitutional effect were 372, 268, and 105 kJ/mole (89, 64, and 25 kcal/mole), respectively.

e. For Co-base source/alloy X sink couples, the average total and diffusion activation energies and the average constitutional effect were 343, 286, and 57 kJ/mole (82, 68.4, and 13.6 kcal/mole), respectively.

f. For the Ni-base couples the average diffusion-zone diffusion coefficients were 8.3×10^{-11} cm²/sec at 1095° C and 3.8×10^{-10} cm²/sec at 1205° C.

g. For the Co-base source/alloy X sink couples the average diffusion-zone diffusion coefficients were 1.0×10^{-10} cm²/sec at 1095° C and 8.1×10^{-10} cm²/sec at 1205° C.

h. For the Co-base source/Co-base sink couple the diffusion-zone diffusion coefficient was 9.4×10^{-11} cm²/sec at 1095° C.

3. Additional results:

a. The Co-rich corner of the ternary Co-Cr-Al system was constructed at 1100° C from β -phase volume fraction data, and a partial 1200° C diagram was also constructed.

b. A rule-of-mixtures microhardness law was obeyed by the bulk β -containing MCrAl alloys examined after 500-hour, 1095^o C anneals with average microhardness proportional to the volume percent of β .

Lewis Research Center,
National Aeronautics and Space Administration,
and
U. S. Army Air Mobility R&D Laboratory,
Cleveland, Ohio, August 12, 1976,
505-01.

REFERENCES

1. Taylor, A.; and Floyd, R. W.: The Constitution of Nickel-Rich Alloys of the Nickel-Chromium-Aluminum System. *J. Inst. Metals*, vol. 81, 1952-53, pp. 451-464.
2. Goward, G. W.: Current Research on the Surface Protection of Superalloys for Gas Turbine Engines. *J. Metals*, vol. 22, no. 10, Oct. 1970, pp. 31-39.
3. Felten, E. J.; Strangman, T. E.; and Ulion, N. E.: Coatings for Directional Eutectics. (PWA-5091, Pratt & Whitney Aircraft; NAS3-16792) NASA CR-134735, 1974.
4. Levinstein, Moses A.: Enriched Aluminide Coatings for Dispersion Strengthened Nickel Materials. (General Electric Co.; NAS3-14314) NASA CR-121250, 1973.
5. Smialek, James L.; and Lowell, Carl E.: Effects of Diffusion on Aluminum Depletion and Degradation of NiAl Coatings. *J. Electrochem. Soc.*, vol. 121, no. 6, June 1974, pp. 800-805.
6. Crank, J.: *The Mathematics of Diffusion*. Oxford University Press (London), 1956, p. 14.
7. Pettit, F. S.: Oxidation Mechanisms for Nickel-Aluminum Alloys at Temperatures Between 900^o and 1300^o C. *Trans. Met. Soc. AIME*, vol. 239, no. 9, Sept. 1967, pp. 1296-1305.
8. Wallwork, G. R.; and Hed, A. Z.: Some Limiting Factors in the Use of Alloys at High Temperatures. *Oxid. Metals*, vol. 3, no. 2, Mar. 1971, pp. 171-184.
9. Janssen, M. M. P.: Diffusion in the Nickel-Rich Part of the Ni-Al System at 1000^o to 1300^o C; Ni₃Al Layer Growth, Diffusion Coefficients, and Interface Concentrations. *Met. Trans.*, vol. 4, no. 6, June 1973, pp. 1623-1633.

10. Lowell, Carl E.; Garlick, Ralph G.; and Henry, Bert: Thermal Expansion in the Ni-Cr-Al and Co-Cr-Al Systems to 1200^o C. NASA TM X-3268, 1975.
11. Barrett, Charles A.; and Lowell, Carl E.: Resistance of Nickel-Chromium-Aluminum Alloys to Cyclic Oxidation at 1100^o and 1200^o C. NASA TN D-8255, 1976.
12. Hansen, Max: Constitution of Binary Alloys. 2nd ed., McGraw-Hill Book Co., Inc., 1958.
13. Westbrook, J. H.: Temperature Dependence of Hardness of the Equi-Atomic Iron Group Aluminides. J. Electrochem. Soc., vol. 103, no. 1, Jan. 1956, pp. 54-63.
14. Smialek, James L.; and Hehemann, Robert F.: Transformation Temperatures of Martensite in β -Phase Nickel Aluminide. Met. Trans., vol. 4, no. 6, June 1973, pp. 1571-1575.
15. Jost, Wilhelm: Diffusion in Solids, Liquids, and Gases. Academic Press, Inc., 1952, pp. 72-73.
16. Askill, John: Tracer Diffusion Data for Metals, Alloys, and Simple Oxides. IFI/Plenum Data Corp., 1970, pp. 27-36.
17. Swalin, R. A.; and Martin, Allan: Solute Diffusion in Nickel-Base Substitutional Solid Solutions. J. Met., vol. 8, no. 5, May 1956, pp. 567-572.
18. Hancock, G. F.: Diffusion of Nickel in Alloys Based on the Intermetallic Compound Ni₃Al (γ'). Phys. Stat. Sol. (A), vol. 7, 1971, pp. 535-540.

TABLE I. - ALLOY CHEMISTRIES

Alloy	Phases present as cast ^a	Weight percent				Atomic percent				Volume percent β in bulk ^b
		Co	Ni	Cr	Al	Co	Ni	Cr	Al	
Nickel-base alloys										
X	γ	----	90.0	10.0	----	----	89.0	11.0	----	---
1C	$\beta + \gamma + \gamma' + \alpha$	----	72.4	14.9	12.7	----	61.9	14.4	23.7	70
2C	$\gamma + \beta + \gamma' + \alpha$	----	75.5	12.8	11.7	----	65.4	12.5	22.0	40
3S	$\gamma' + \gamma$	----	81.3	12.7	6.0	----	74.7	13.2	12.1	---
4S	$\gamma + \gamma'$	----	76.7	17.7	5.5	----	70.5	18.4	11.1	---
5C	$\beta + \gamma + \alpha$	----	66.0	18.3	15.7	----	54.6	17.1	28.2	96
6C	$\beta + \gamma + \alpha + \gamma'$	----	67.9	19.5	12.6	----	57.9	18.8	23.4	65
7S	γ	----	82.5	14.7	2.8	----	78.4	15.8	5.8	---
8C	$\gamma + \beta + \alpha + \gamma'$	----	70.4	20.8	8.8	----	62.3	20.8	16.9	25
9C	$\gamma' + \gamma$	----	81.6	9.6	8.8	----	73.1	9.7	17.2	---
β	β	----	68.6	----	31.4	----	50.1	----	49.9	100
Cobalt-base alloys										
1'C	$\beta + \alpha\text{Co}$	74.6	----	15.9	9.5	65.8	----	15.9	18.3	60
2'C	$\beta + \alpha\text{Co}$	77.3	----	11.7	11.0	67.5	----	11.6	21.0	80
3'C	$\alpha\text{Co} + \beta$	81.7	----	12.3	6.0	75.1	----	12.9	12.1	10
4'C	$\alpha\text{Co} + \beta$	76.1	----	18.1	5.8	69.6	----	18.8	11.6	20
5'C	$\beta + \alpha\text{Co}$	67.9	----	19.6	12.5	57.8	----	18.9	23.3	80
6'C	$\beta + \alpha\text{Co}$	80.2	----	10.4	9.0	71.3	----	10.5	18.2	55
7'C	$\beta + \alpha\text{Co}$	73.3	----	13.5	13.2	62.4	----	13.1	24.6	85
8'S	αCo	82.7	----	14.7	2.6	78.7	----	15.9	5.4	---
9'C	$\beta + \alpha\text{Co}$	69.1	----	22.1	8.8	60.9	----	22.1	17.0	40

^a Phases listed in descending order of amount present.

^b When annealed at 1095° C for 500 hr.

TABLE II. - DIFFUSION ANNEALS FOR EACH COUPLE TYPE

Temperature, °C	Annealing time, hr ^a			
	100	300	500	500 + 5 hr at 1095° C
1000			x ^b	
1095	x ^b	x	x	
1150			x ^b	x
1205	x ^b	x	x	x

^a Total times including adjustment for diffusion bonding. To obtain actual annealing times subtract 2 hr at 1000° C, 1 hr at 1095° C, and 1/2 hr at 1150° C.

^b Co-base and Ni-base couples had ZrO₂-12Y₂O₃ intentional markers at weld interfaces as assembled.

TABLE IV. - ESTIMATED COATING LIFE
 BASED ON DIFFUSION

Couple	Coating thickness, cm	Annealing temperature, °C	
		1095	1205
		Life, hr ^a	
1C/X	0.013 ↓ .0063 ↓ .013 ↓	>430	>62
2C/X		>130	>18
5C/X		^b >2400	^b 310
6C/X		^b >1100	^b 67
8C/X		>73	7
8C/4S		>340	20
5C/7S		----	^b 660
2C/3S		>290	----
β/X		^c 150	^c 10
1'C/X		390	<34
2'C/X		<470	<39
3'C/X		110	----
4'C/X		180	<10
5'C/X		700	<77
6'C/X		<310	<29
7'C/X		<630	<65
9'C/X		470	<36
4'C/8'S		960	<22
9'C/9C	430	<36	

^a> indicates conservative life estimate and < indicates unconservative life estimate with respect to cyclic oxidation performance.

^bLife estimates based on rate constant for β recession which is influenced by the faster $\beta + \alpha + \gamma \rightarrow \beta + \gamma$ reaction. At 1095° C this reaction is slow enough to reduce k, but at 1205° C the effect is small.

^cLife based on growth of martensitic β.

TABLE V. - ANALYSIS OF LAYER GROWTH DATA

Couple	Annealing temperature, °C								
	1095				1205				
	β Source strength, B	β Recession rate constant, k, cm ² /sec	Dimensionless parameter, g	Interdiffusion coefficient, D, cm ² /sec	β Source strength, B	β Recession rate constant, k, cm ² /sec	Dimensionless parameter, g	Interdiffusion coefficient, D, cm ² /sec	
Nickel-base couples									
1C/X	0.26	1.1×10 ⁻¹⁰	0.65	6.5×10 ⁻¹¹	0.23	7.6×10 ⁻¹⁰	0.70	3.9×10 ⁻¹⁰	
2C/X	.15	3.6×10 ⁻¹⁰	.86	1.2×10 ⁻¹⁰	.11	2.6×10 ⁻⁹	.97	6.9×10 ⁻¹⁰	
5C/X	.44	2.0×10 ⁻¹¹	.42	2.8×10 ⁻¹¹	.41	1.5×10 ⁻¹⁰	.45	1.9×10 ⁻¹⁰	
6C/X	.36	4.4×10 ⁻¹¹	.51	4.2×10 ⁻¹¹	.29	7.0×10 ⁻¹⁰	.60	4.9×10 ⁻¹⁰	
8C/X	.12	6.4×10 ⁻¹⁰	.94	1.8×10 ⁻¹⁰	.045	6.8×10 ⁻⁹	1.26	1.1×10 ⁻¹⁰	
5C/7S	.59	3.6×10 ⁻¹³	.28	1.1×10 ⁻¹²	.53	7.1×10 ⁻¹¹	.33	1.1×10 ⁻¹⁰	
2C/3S	.33	1.6×10 ⁻¹⁰	.55	1.3×10 ⁻¹⁰	-----	-----	-----	-----	
8C/4S	.31	1.4×10 ⁻¹⁰	.58	1.0×10 ⁻¹⁰	.11	2.3×10 ⁻⁹	.97	6.1×10 ⁻¹⁰	
				$\bar{D} = 8.3 \times 10^{-11}$					$\bar{D} = 3.8 \times 10^{-10}$
Cobalt-base source/alloy X (Ni-10Cr) sink couples									
1'C/X	0.34	1.2×10 ⁻¹⁰	0.54	1.0×10 ⁻¹⁰	0.25	1.4×10 ⁻⁹	0.66	8.0×10 ⁻¹⁰	
2'C/X	.39	1.0×10 ⁻¹⁰	.44	1.3×10 ⁻¹⁰	.30	1.2×10 ⁻⁹	.59	8.6×10 ⁻¹⁰	
3'C/X	.11	4.1×10 ⁻¹⁰	.97	1.1×10 ⁻¹⁰	-----	-----	-----	-----	
4'C/X	.15	2.6×10 ⁻¹⁰	.86	8.8×10 ⁻¹¹	.02	4.7×10 ⁻⁹	1.15	8.9×10 ⁻¹⁰	
5'C/X	.46	6.7×10 ⁻¹¹	.40	1.0×10 ⁻¹⁰	.39	6.1×10 ⁻¹⁰	.44	7.9×10 ⁻¹⁰	
6'C/X	.29	1.5×10 ⁻¹⁰	.60	1.0×10 ⁻¹⁰	.19	1.6×10 ⁻⁹	.77	6.7×10 ⁻¹⁰	
7'C/X	.46	7.5×10 ⁻¹¹	.40	1.2×10 ⁻¹⁰	.39	7.2×10 ⁻¹⁰	.44	9.3×10 ⁻¹⁰	
9'C/X	.34	1.0×10 ⁻¹⁰	.54	8.6×10 ⁻¹¹	.24	1.3×10 ⁻⁹	.68	7.0×10 ⁻¹⁰	
				$\bar{D} = 1.0 \times 10^{-10}$					$\bar{D} = 8.1 \times 10^{-10}$
Cobalt-base couple									
4'C/8'S	0.49	4.9×10 ⁻¹¹	0.36	9.4×10 ⁻¹¹	0.05	2.1×10 ⁻⁹			

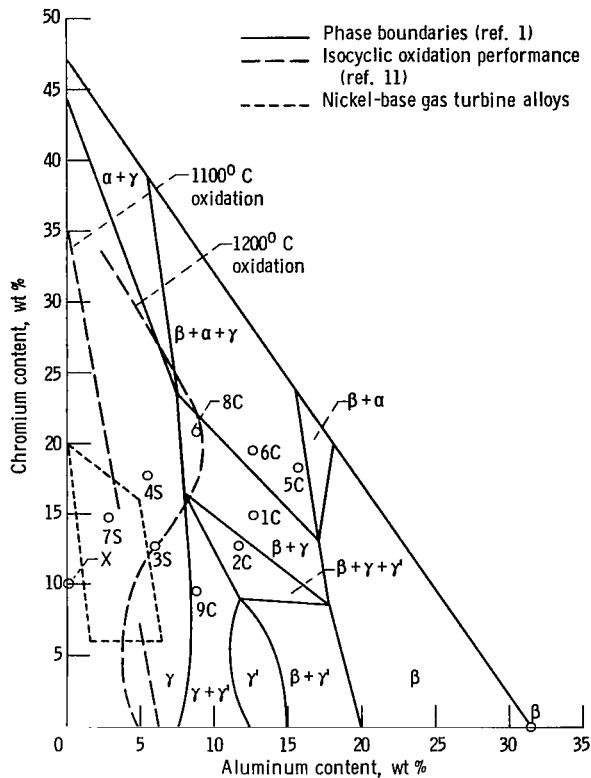


Figure 1. - Ni-Cr-Al equilibrium diagram at 1100^o C showing compositions of alloys in this study and general area in which nickel-base turbine blade and vane alloys fall in terms of their chromium and aluminum contents. (Isocyclic oxidation performance curves at 1100^o and 1200^o C (ref. 11) are also shown.)

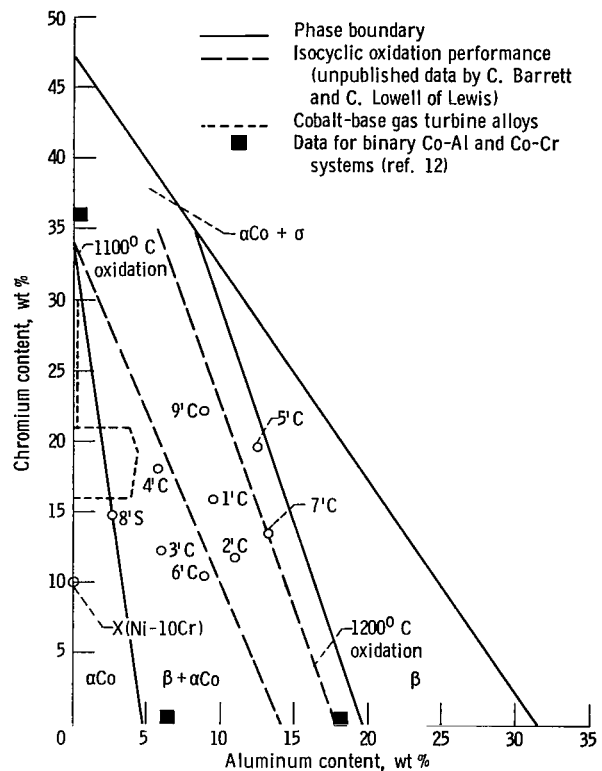
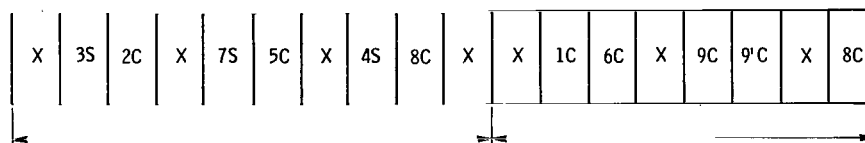
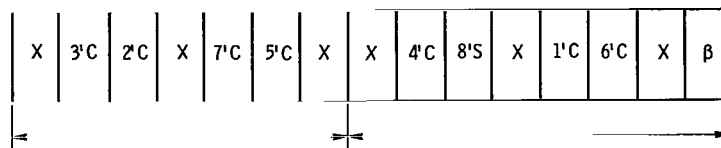


Figure 2. - Approximate Co-Cr-Al equilibrium diagram at 1100^o C (ref. 8) showing compositions of alloys in this study and general area in which cobalt-base high-temperature gas turbine alloys fall in terms of their chromium and aluminum contents. (Isocyclic oxidation performance curves at 1100^o and 1200^o C and data from binary Co-Al and Co-Cr equilibrium diagrams at 1100^o C (ref. 12) are also shown.)

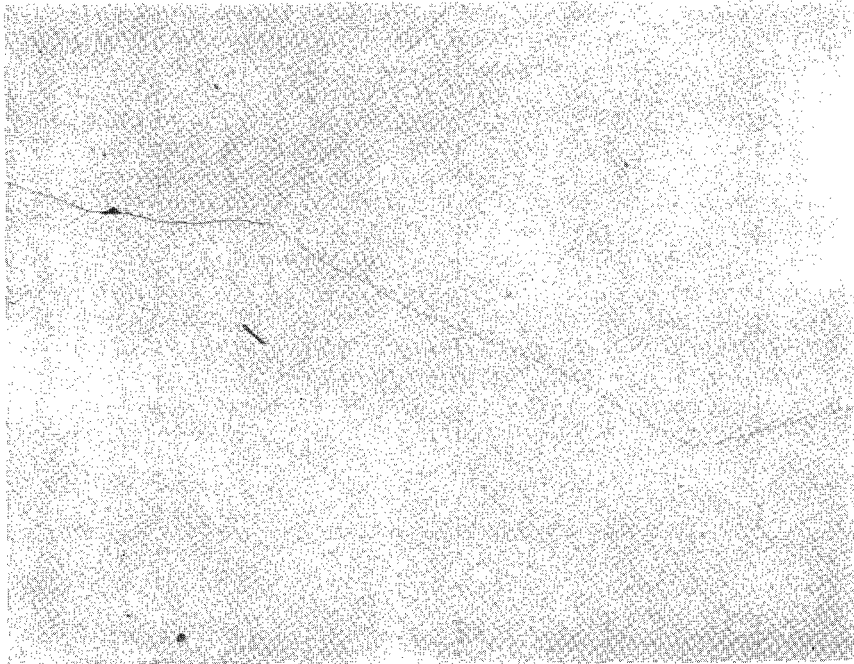


(a) Nickel couples.

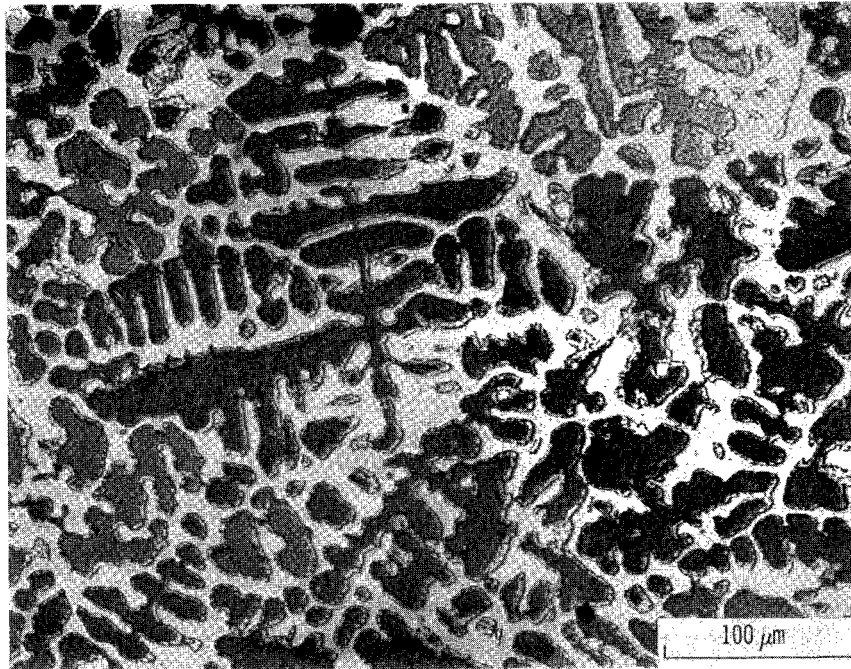


(b) Cobalt couples.

Figure 3. - Diffusion couple assemblies.

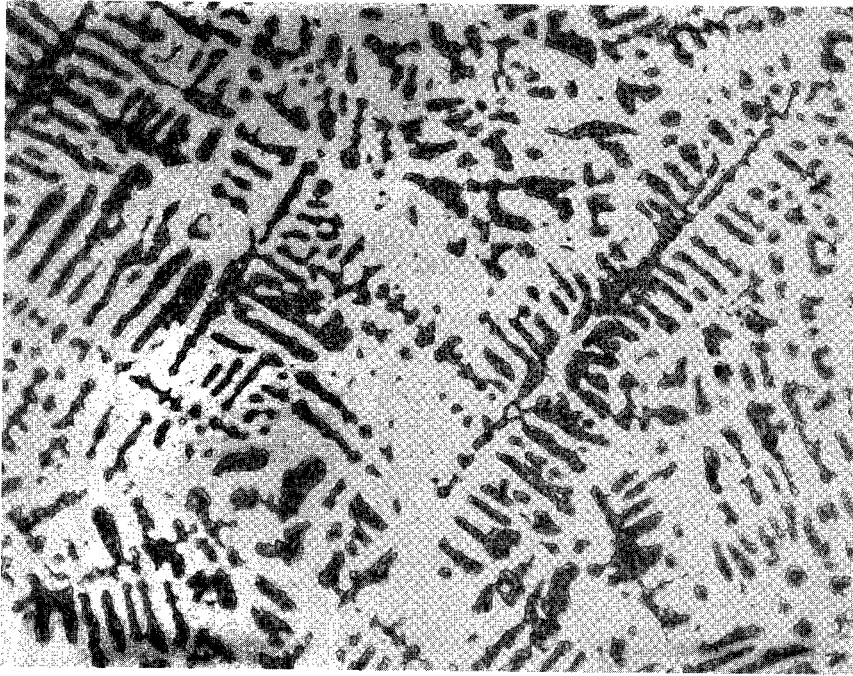


(a) Alloy X: Ni-10Cr, γ .

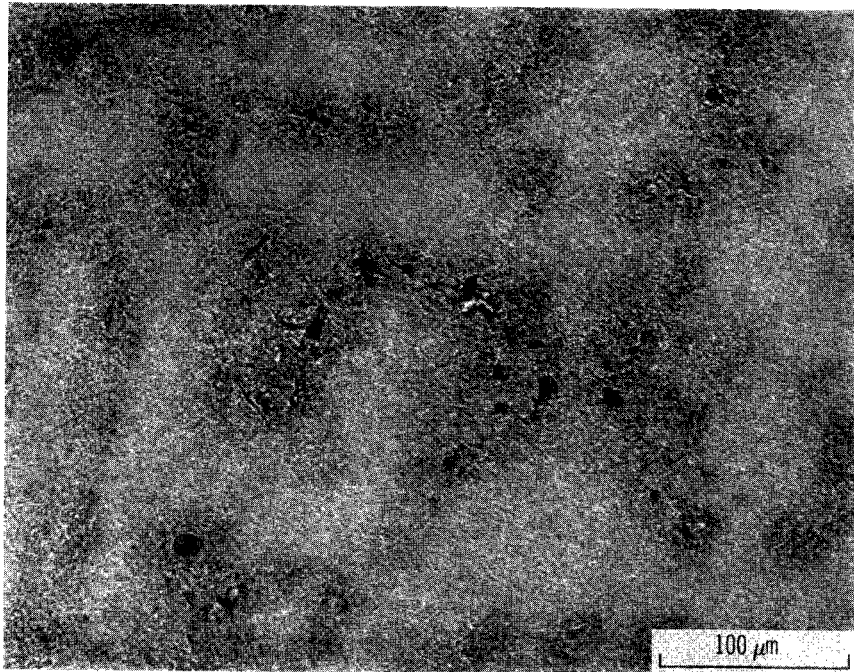


(b) Alloy 1C: Ni-14.9Cr-12.7Al, $\beta + \gamma + \gamma' + \alpha$.

Figure 4. - Microstructures of as-cast nickel-base alloys. (Compositions are in weight percent.)

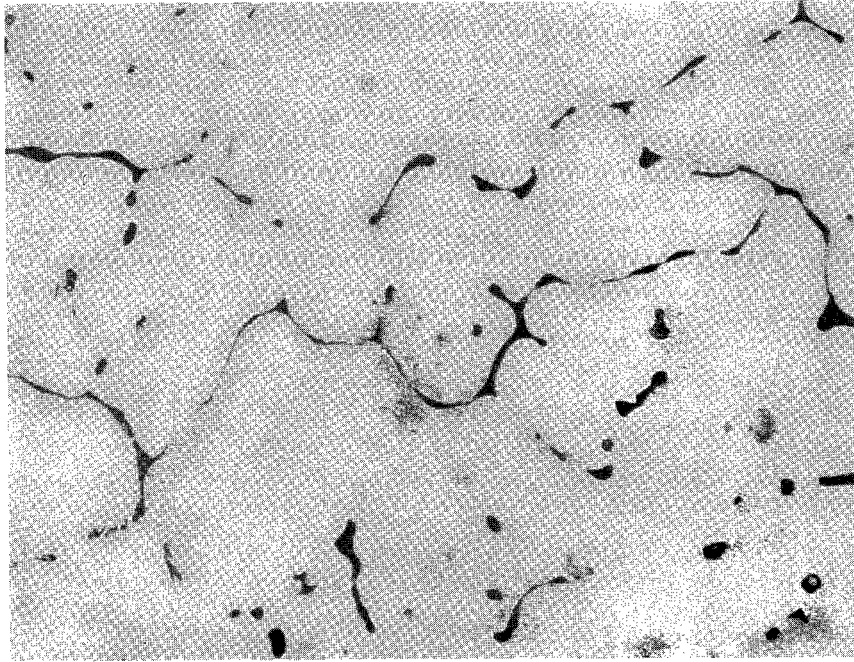


(c) Alloy 2C: Ni-12.8Cr-11.7Al, $\gamma + \beta + \gamma' + \alpha$.

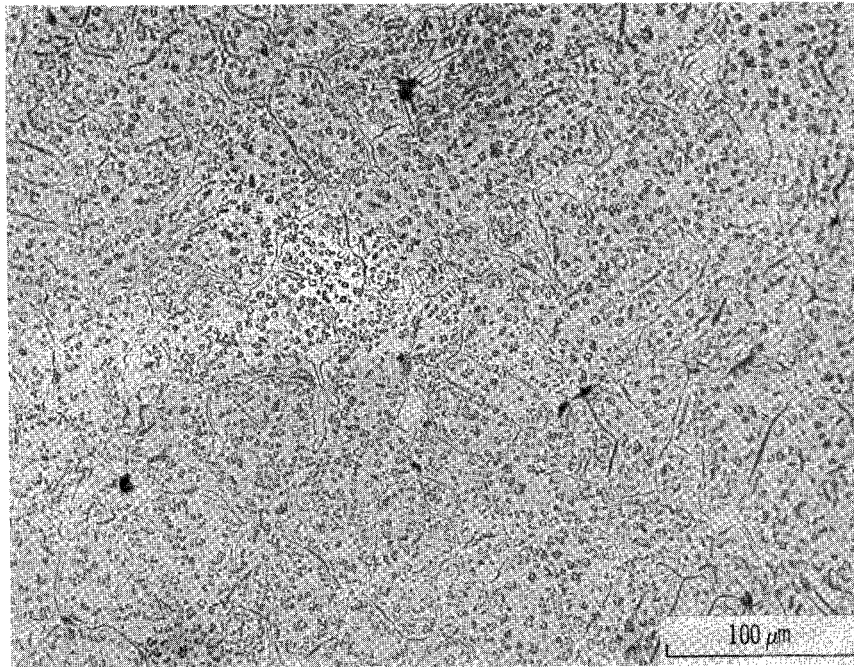


(d) Alloy 3S: Ni-12.7Cr-6.0Al, $\gamma' + \gamma$.

Figure 4. - Continued.

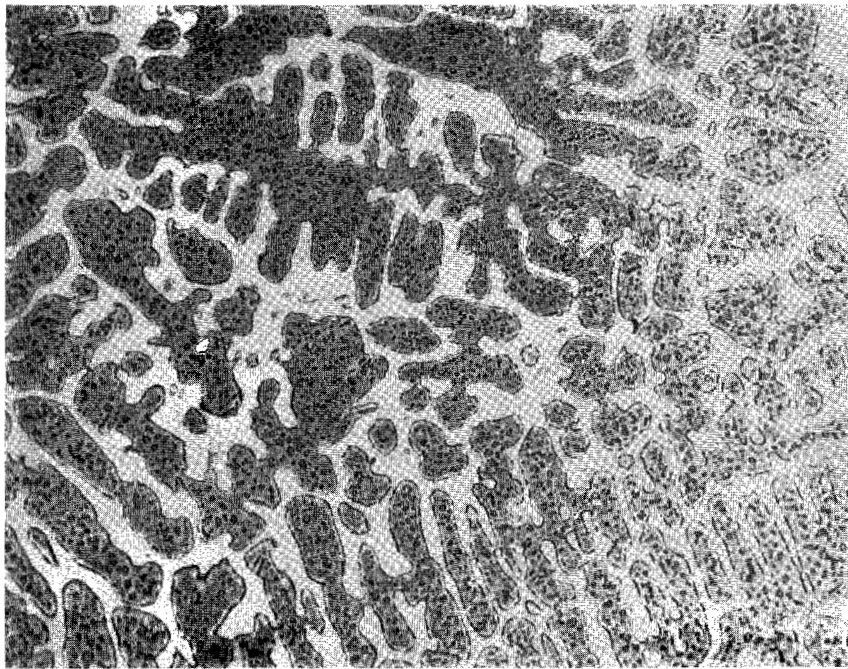


(e) Alloy 4S: Ni-17.7Cr-5.5Al, $\gamma + \gamma'$.

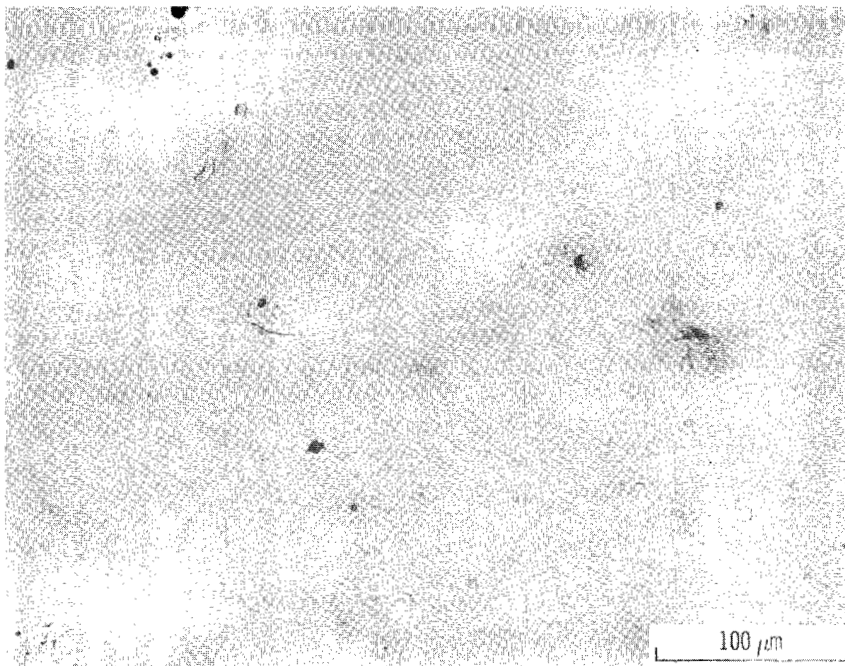


(f) Alloy 5C: Ni-18.3Cr-15.7Al, $\beta + \gamma + \alpha$.

Figure 4. - Continued.

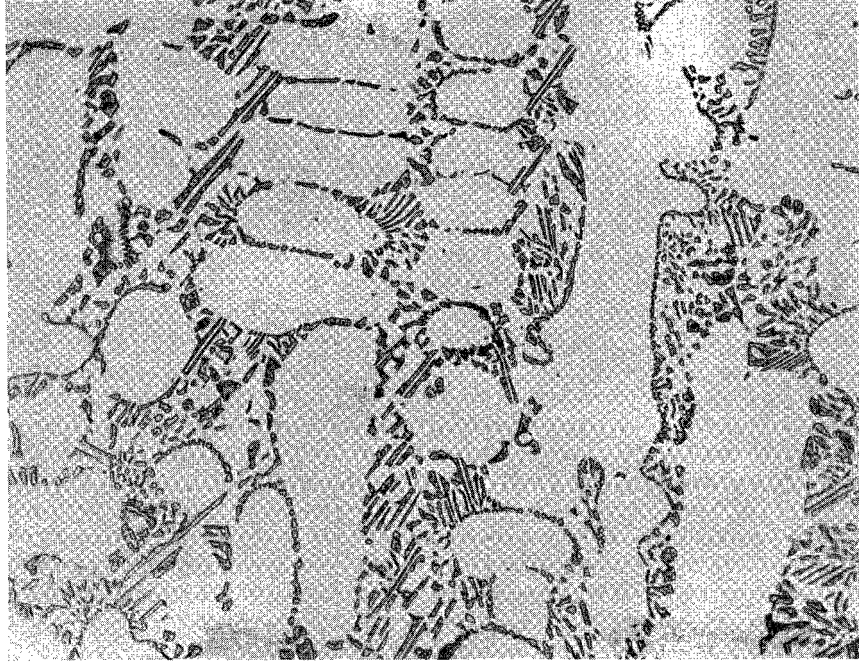


(g) Alloy 6C: Ni-19.5Cr-12.6Al, $\beta+\gamma+a+\gamma'$.

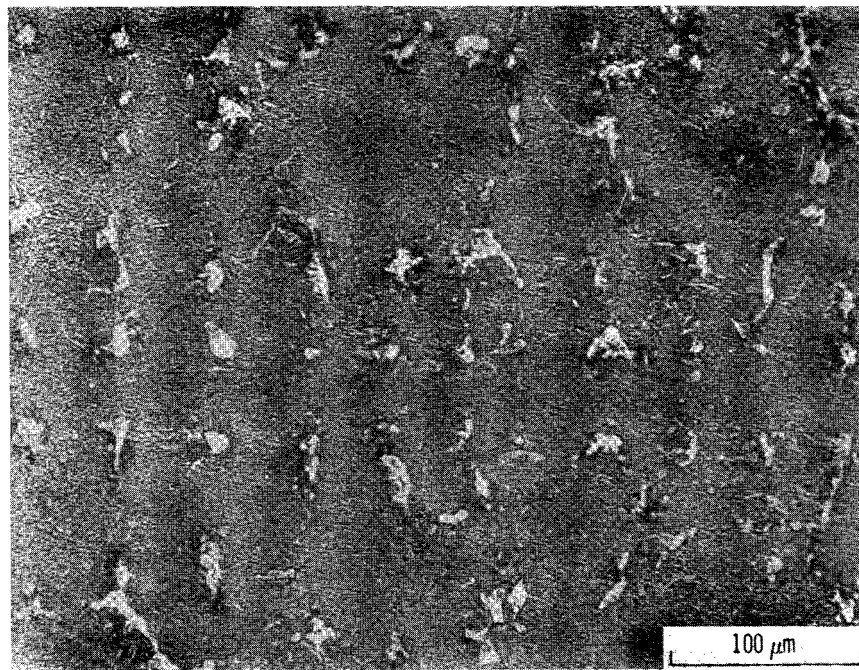


(h) Alloy 7S: Ni-14.7Cr-2.8Al, γ .

Figure 4. - Continued.

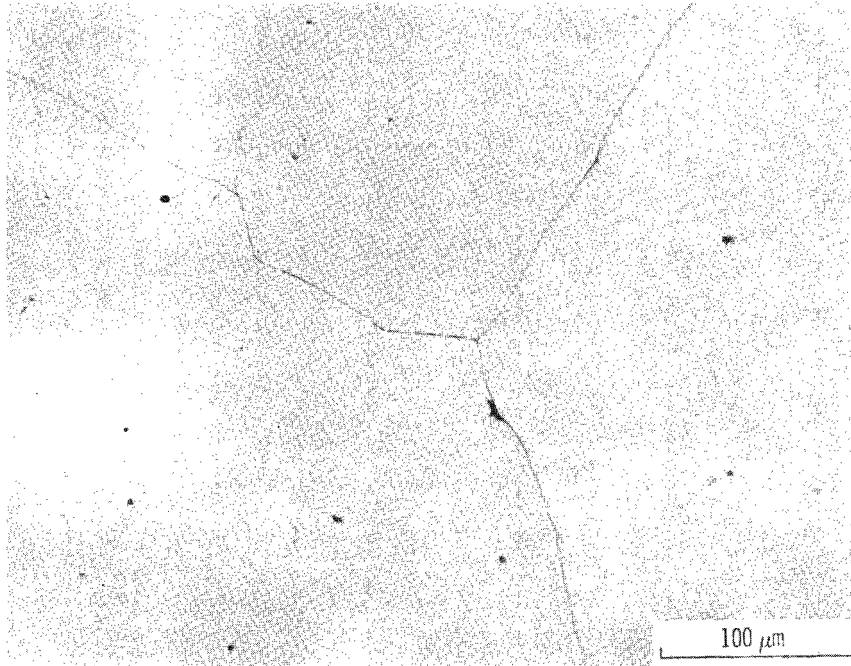


(i) Alloy 8C: Ni-20.8Cr-8.8Al, $\gamma + \beta + \alpha + \gamma'$



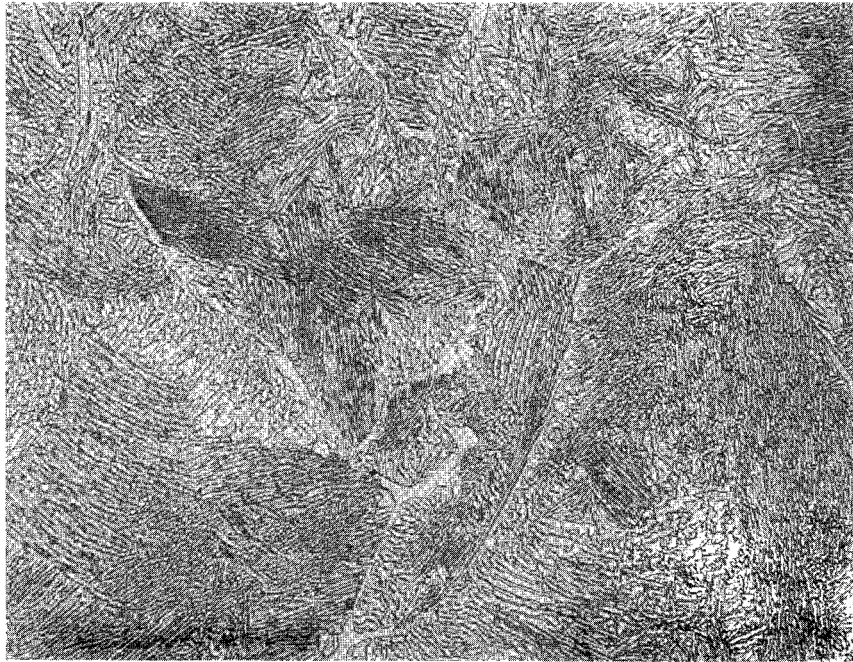
(j) Alloy 9C: Ni-9.6Cr-8.8Al, $\gamma' + \gamma$

Figure 4. - Continued.

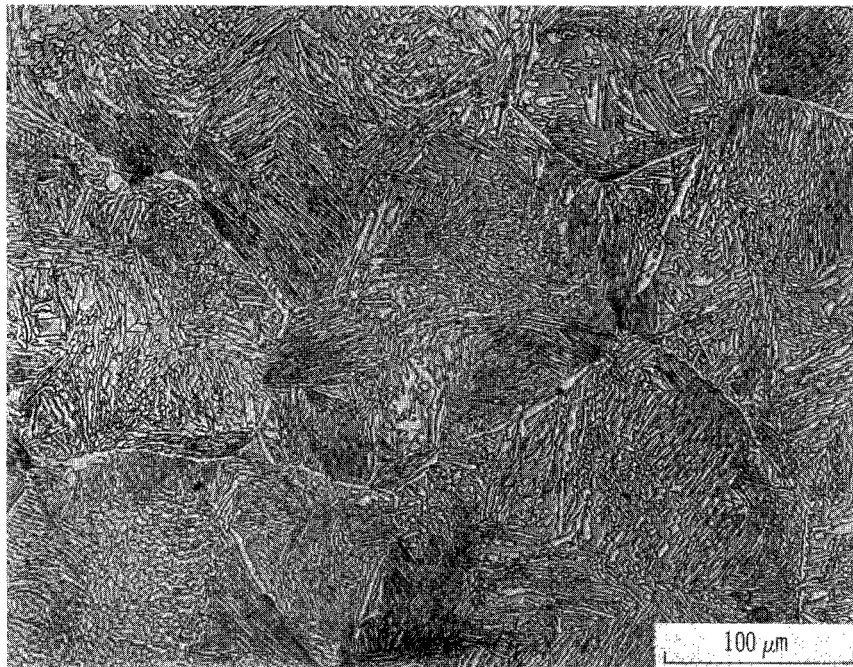


(k) β Alloy: Ni-31.4Al, β .

Figure 4. - Concluded.

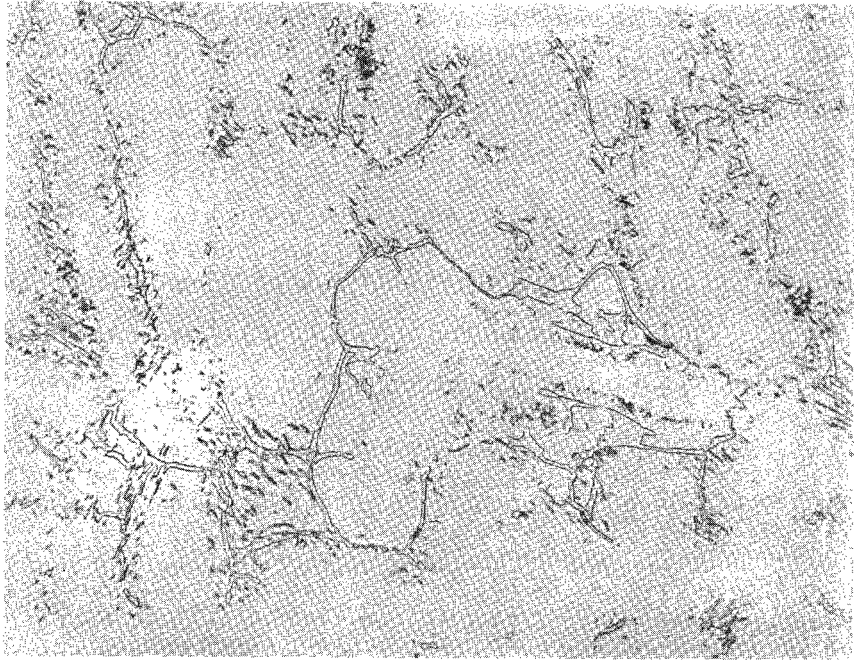


(a) Alloy 1'C: Co-15.9Cr-9.5Al, $\beta + \alpha$ Co.

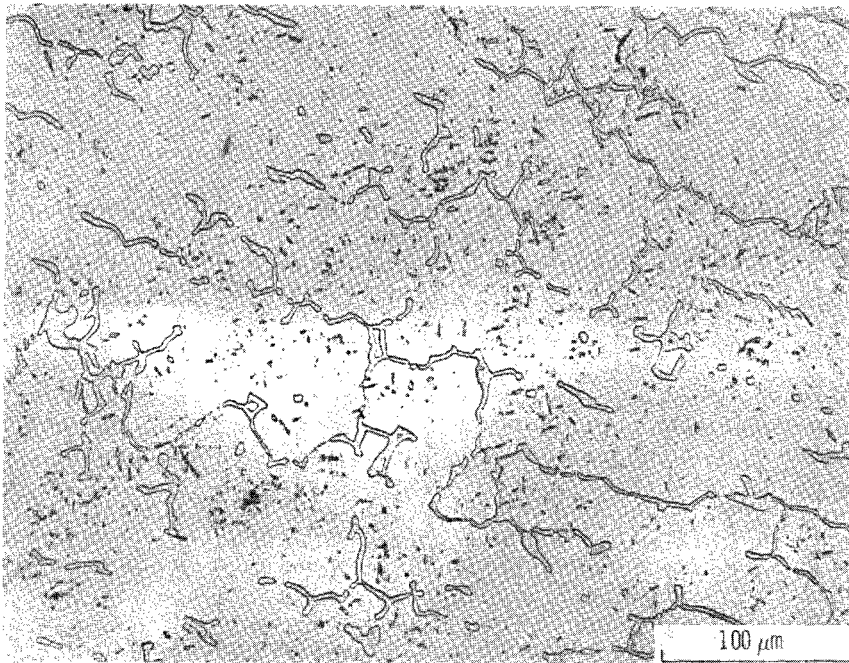


(b) Alloy 2'C: Co-11.7Cr-11.0Al, $\beta + \alpha$ Co.

Figure 5. - Microstructures of as-cast cobalt-base alloys. (Compositions are in weight percent.)

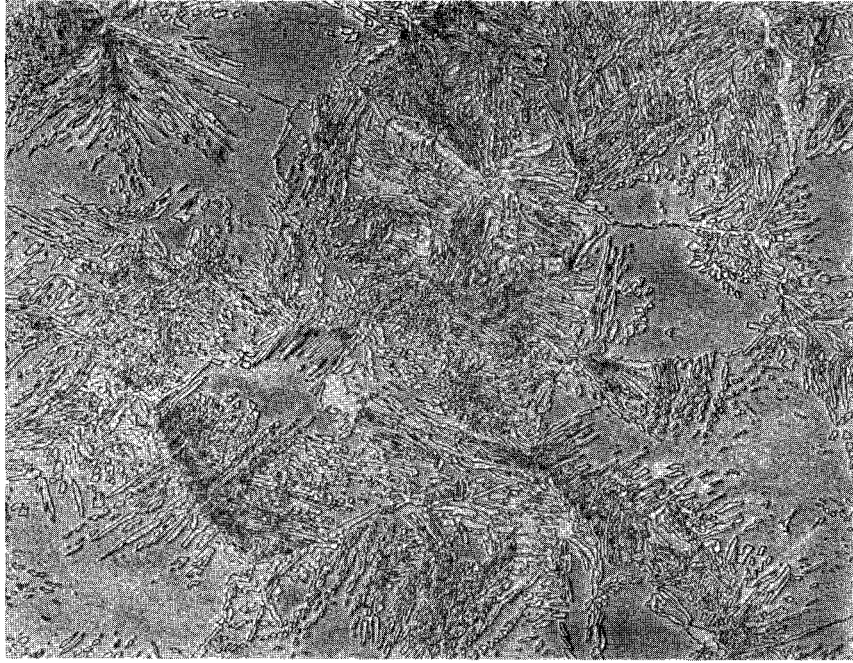


(c) Alloy 3'C: Co-12.3Cr-6.0Al, α Co + β .

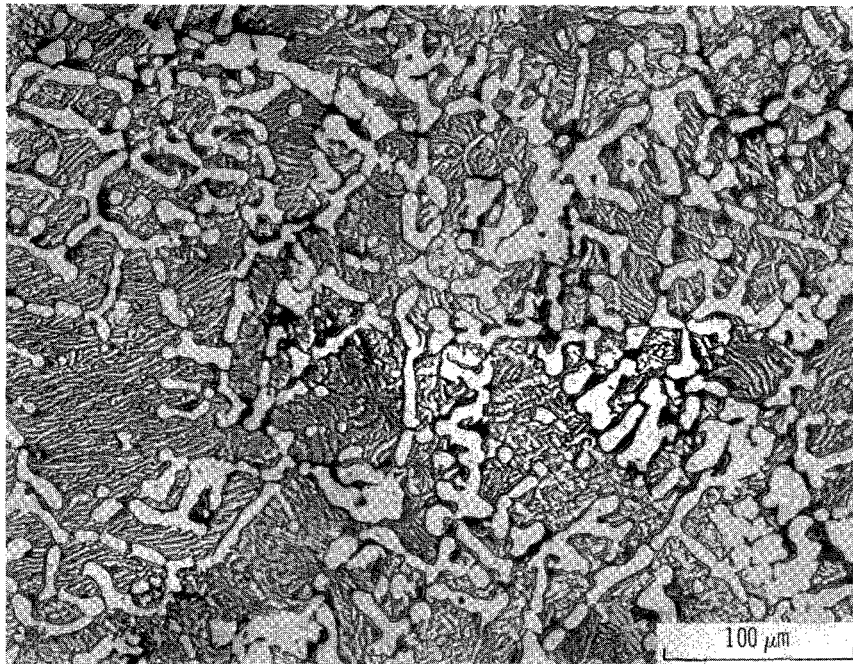


(d) Alloy 4'C: Co-18.1Cr-5.8Al, α Co + β .

Figure 5. - Continued.

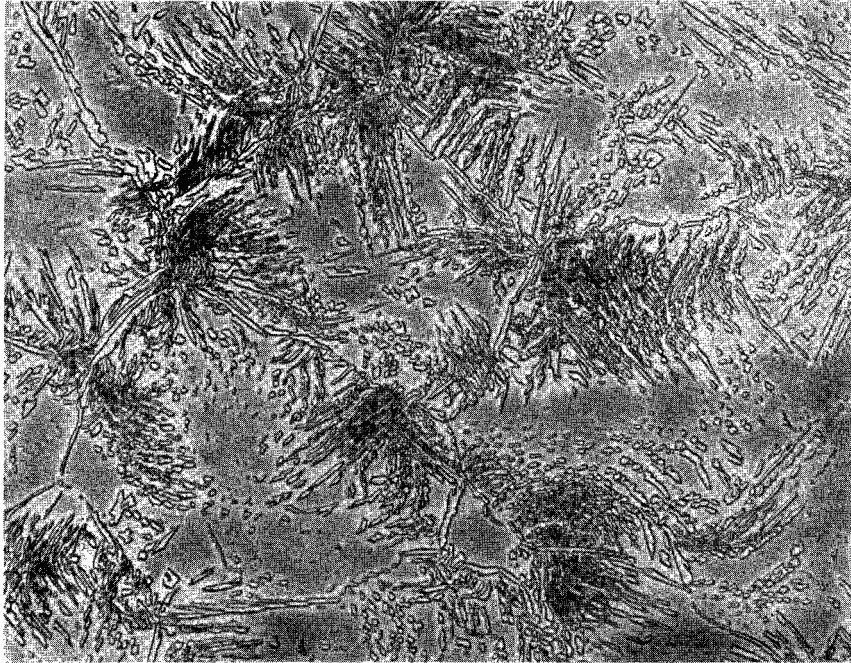


(e) Alloy 5'C: Co-19.6Cr-12.5Al, $\beta + \alpha$ Co.

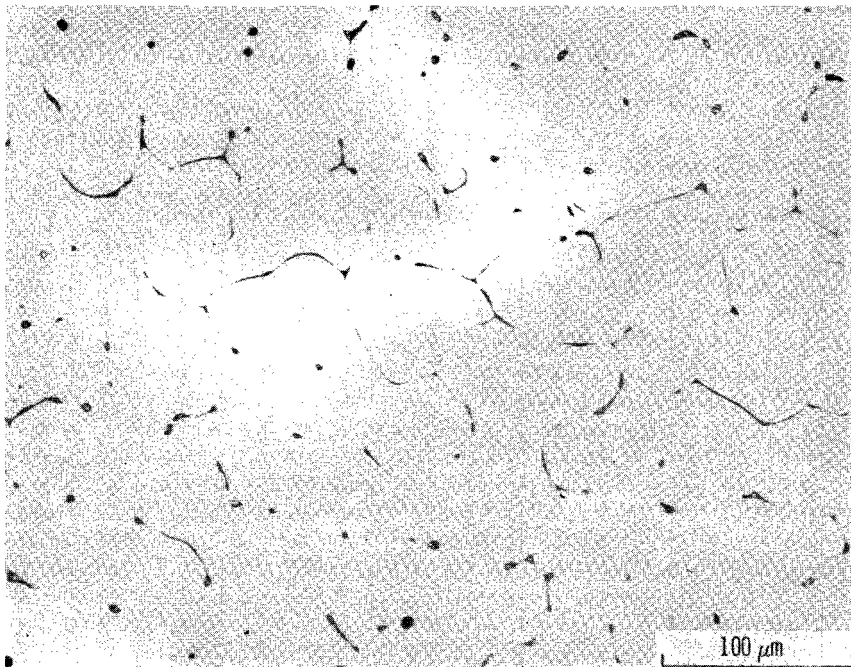


(f) Alloy 6'C: Co-10.4Cr-9.0Al, $\beta + \alpha$ Co.

Figure 5. - Continued.

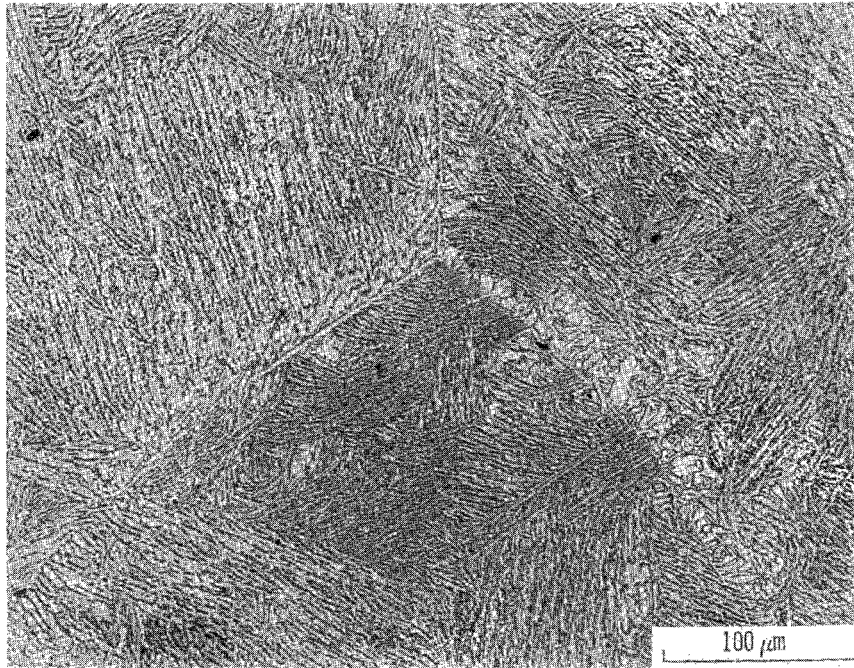


(g) Alloy 7'C: Co-13.5Cr-13.2Al, $\beta + \alpha$ Co.



(h) Alloy 8'S: Co-14.7Cr-2.6Al, α Co.

Figure 5. - Continued.



(i) Alloy 9'C: Co-22.1Cr-8.8Al, $\beta + \alpha$ Co.

Figure 5. - Concluded.

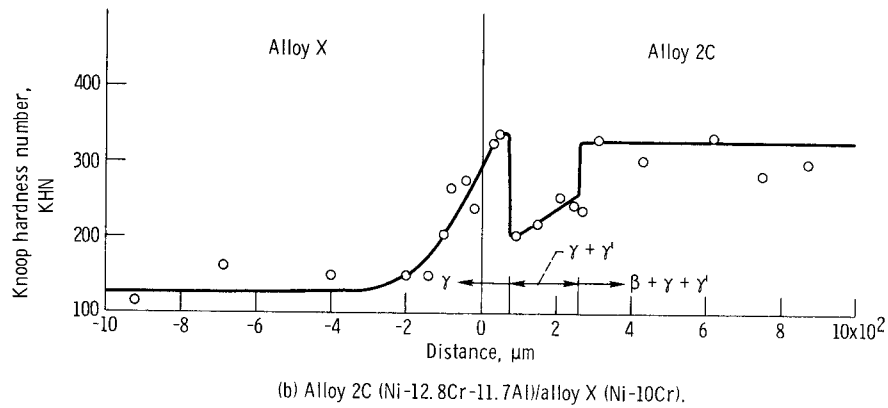
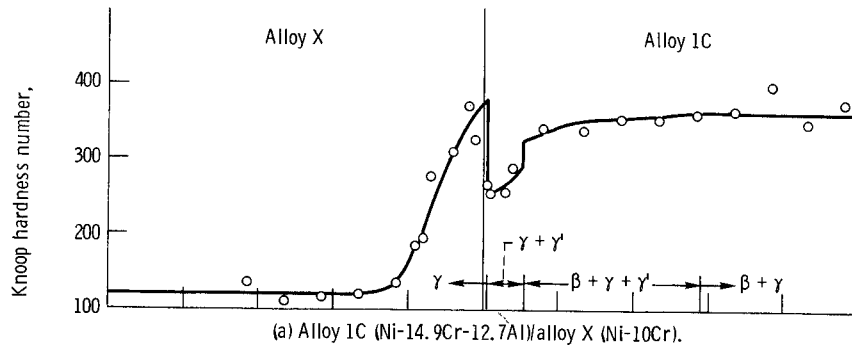
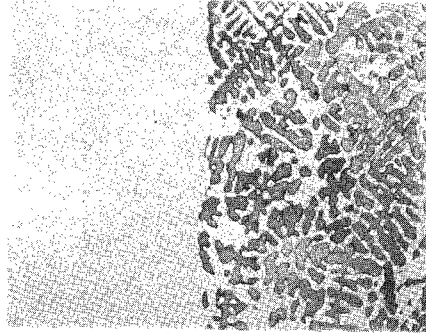


Figure 6. - Microstructures and Knoop microhardness profiles of nickel-base couples annealed for 500 hours at 1095° C.

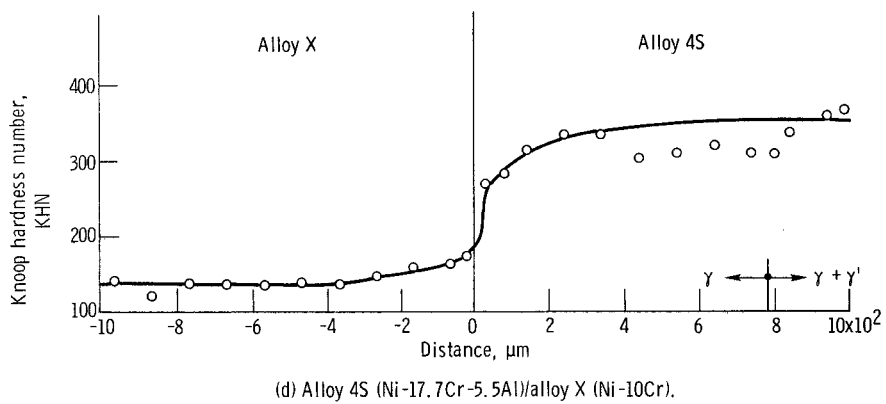
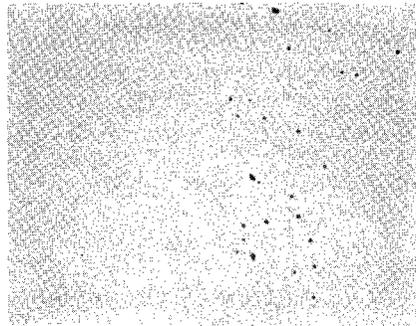
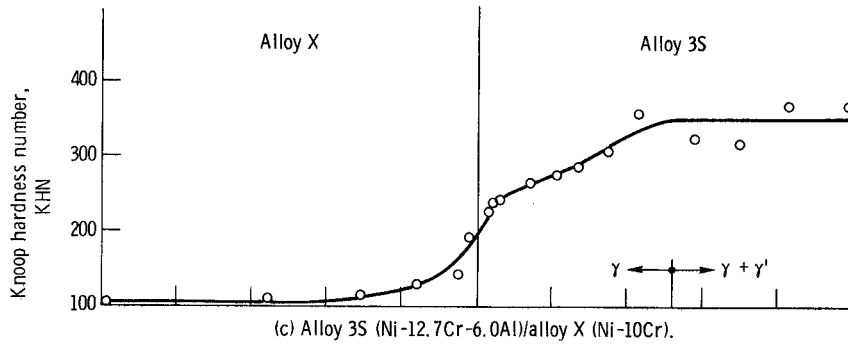
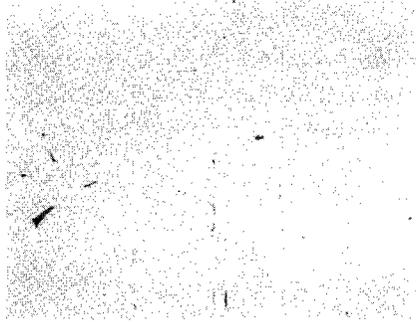
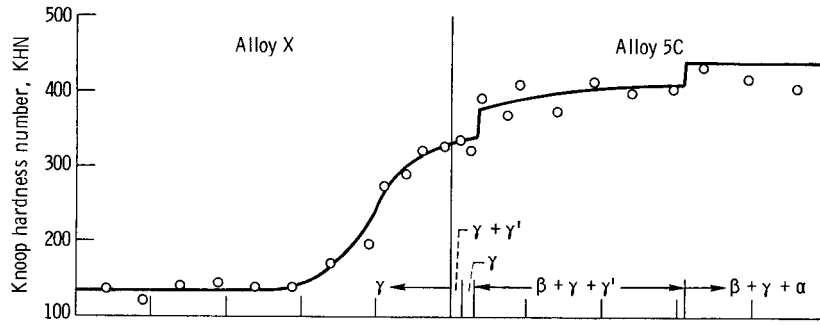
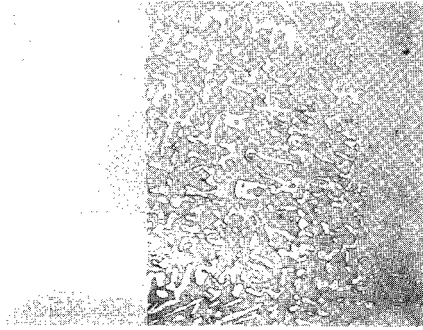
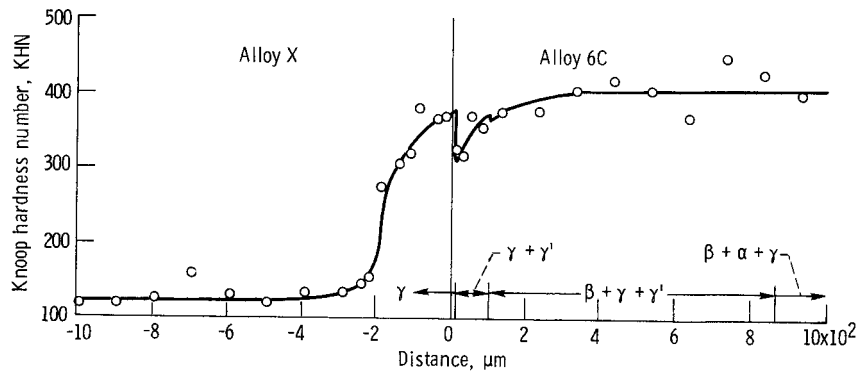
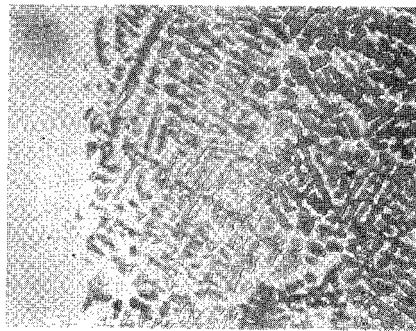


Figure 6. - Continued.



(e) Alloy 5C (Ni-18.3Cr-15.7Al)/alloy X (Ni-10Cr).



(f) Alloy 6C (Ni-19.5Cr-12.6Al)/alloy X (Ni-10Cr).

Figure 6. - Continued.

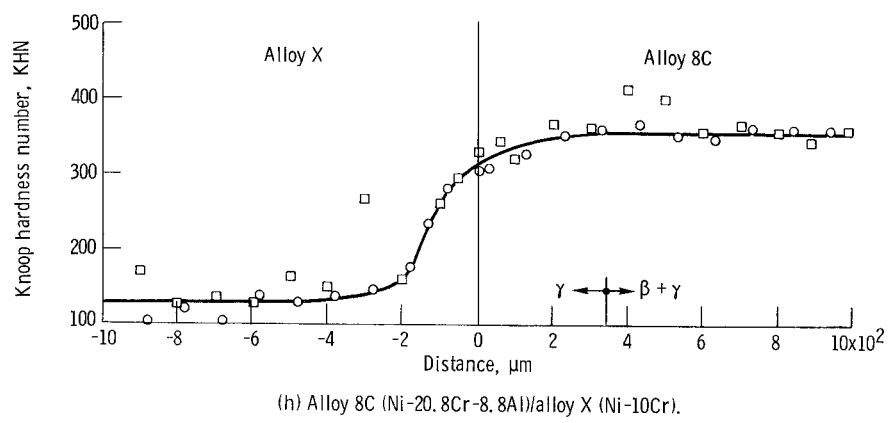
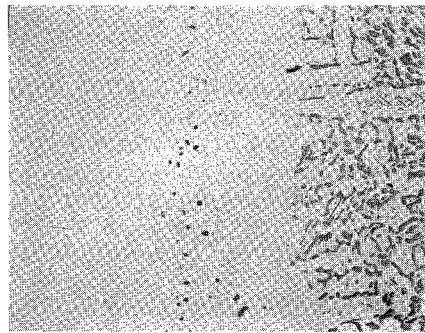
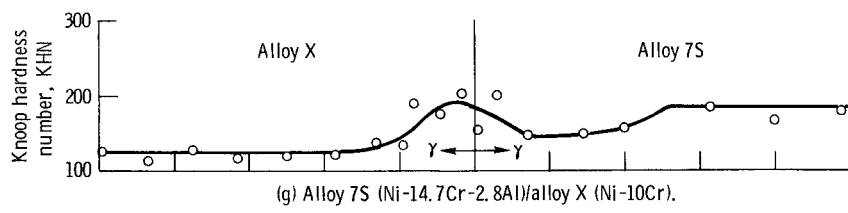
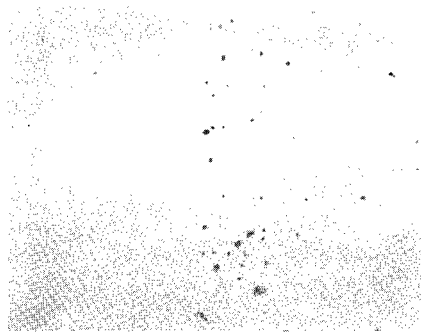


Figure 6. - Continued.

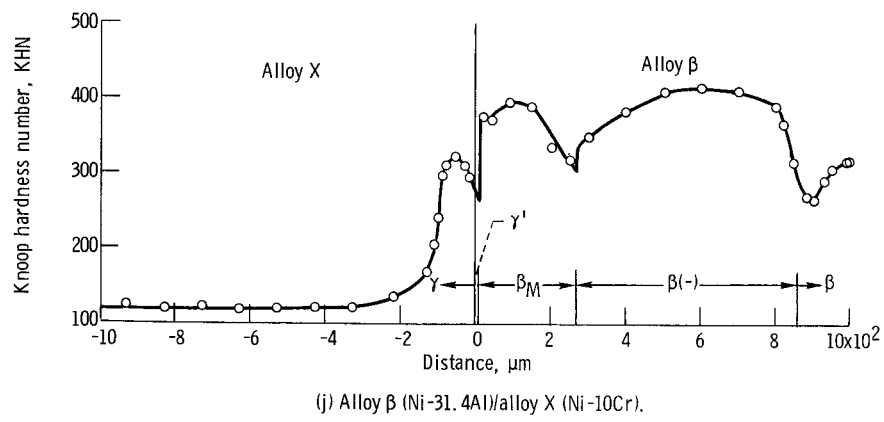
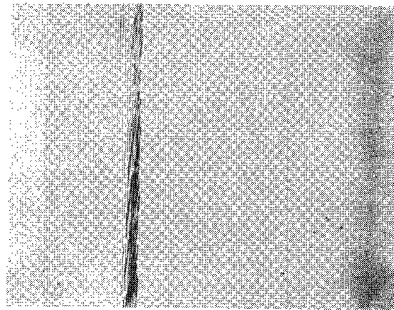
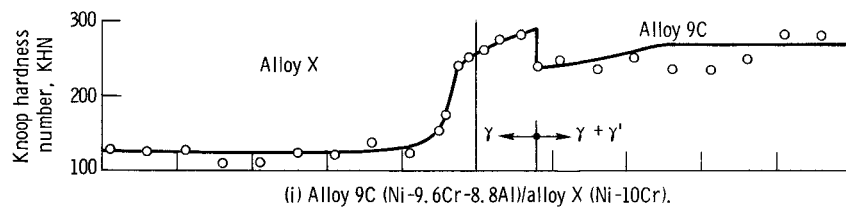
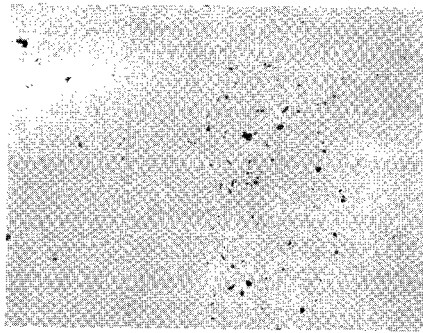


Figure 6. - Continued.

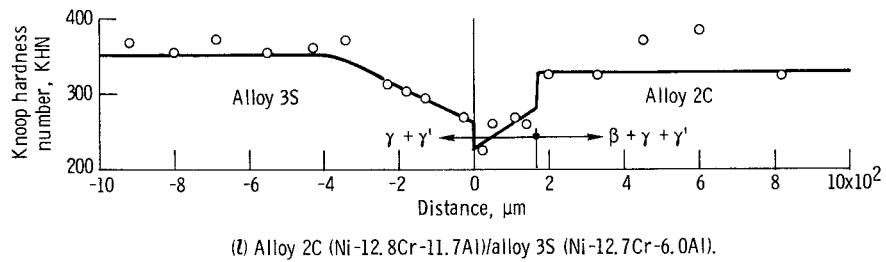
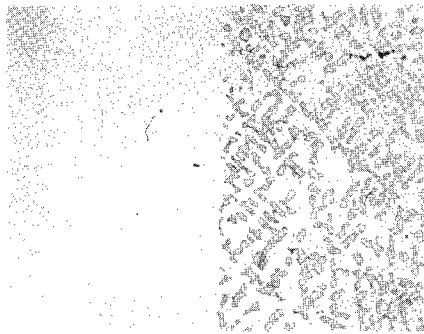
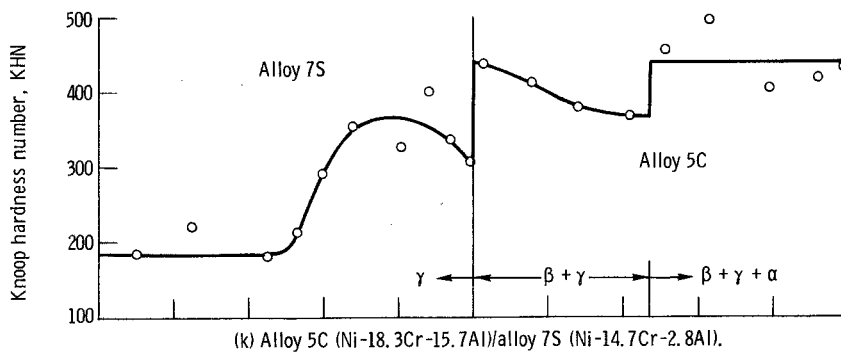
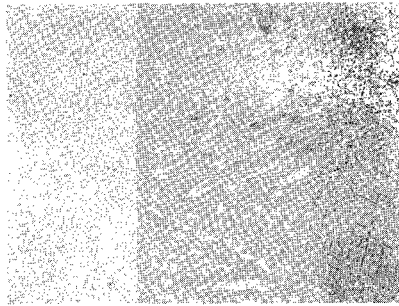


Figure 6. - Continued.

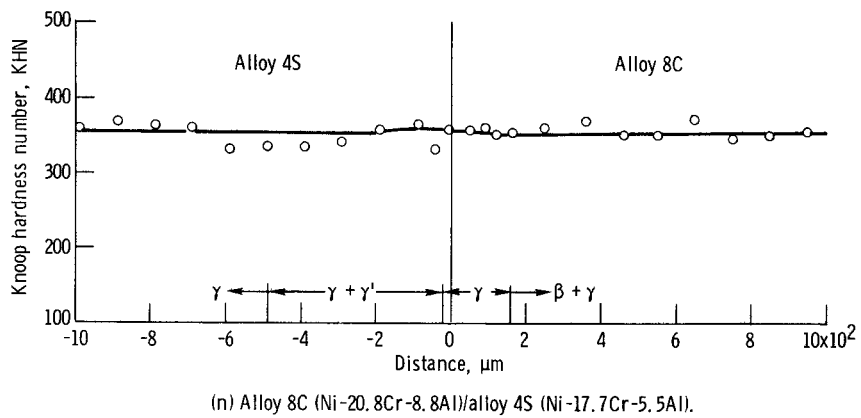
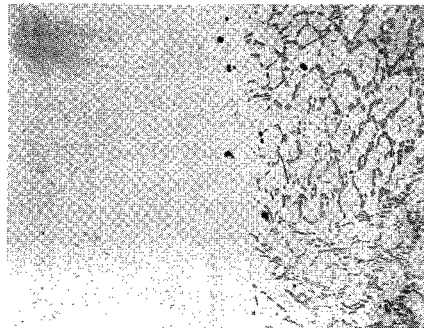
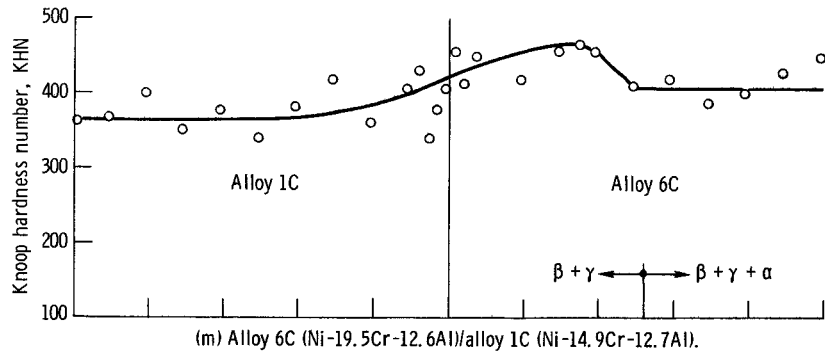
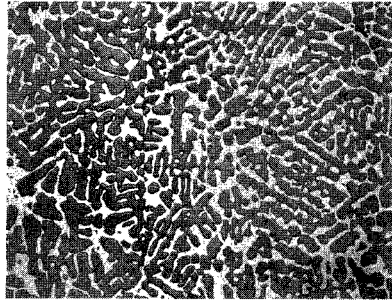


Figure 6. - Concluded.

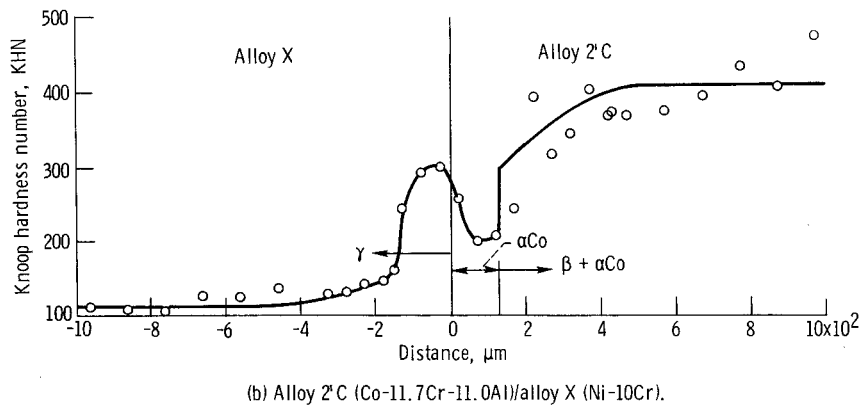
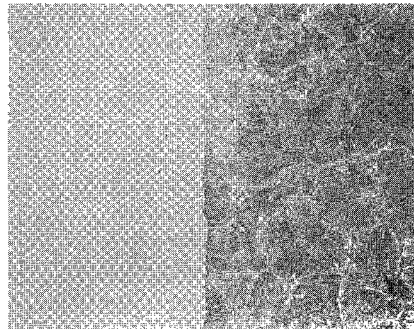
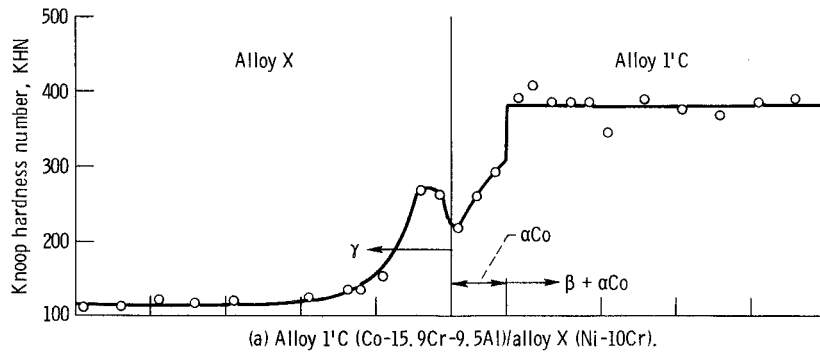
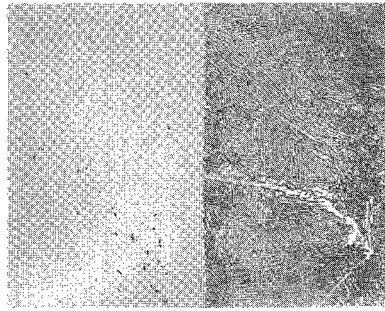
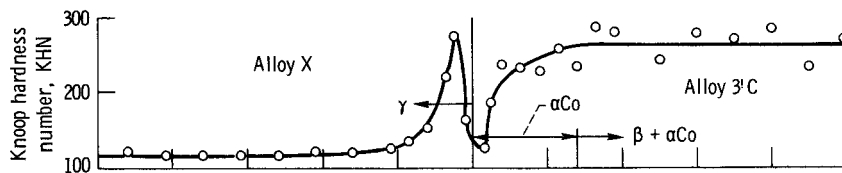
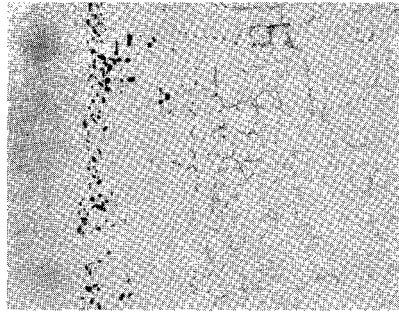
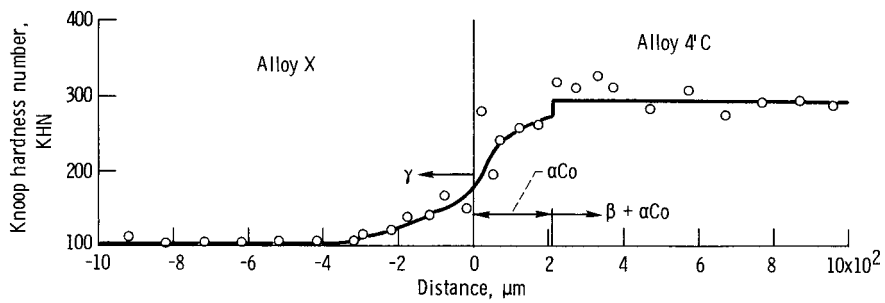
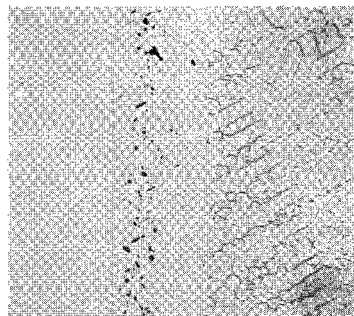


Figure 7. - Microstructures and Knoop microhardness profiles of cobalt-base couples annealed for 500 hours at 1095° C.



(c) Alloy 3'C (Co-12.3Cr-6.0Al)/alloy X (Ni-10Cr).



(d) Alloy 4'C (Co-18.1Cr-5.8Al)/alloy X (Ni-10Cr).

Figure 7. - Continued.

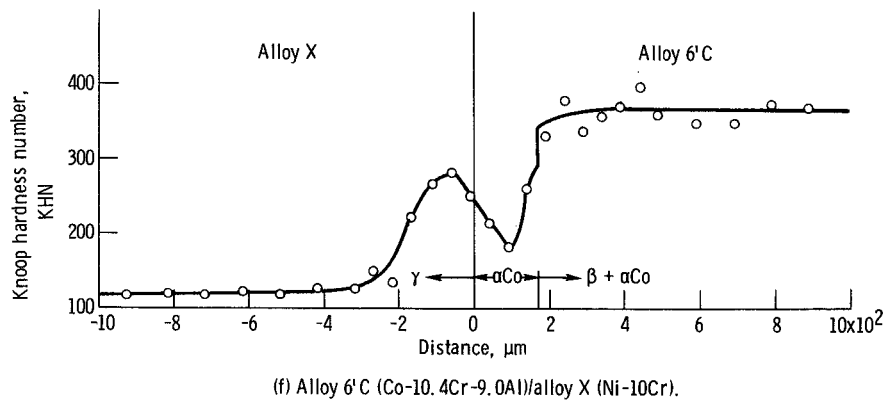
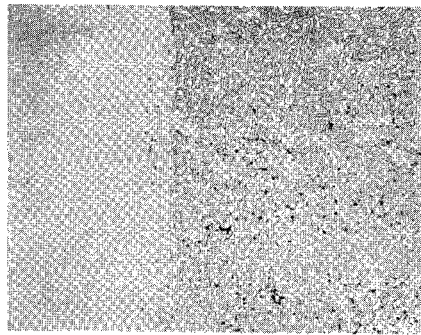
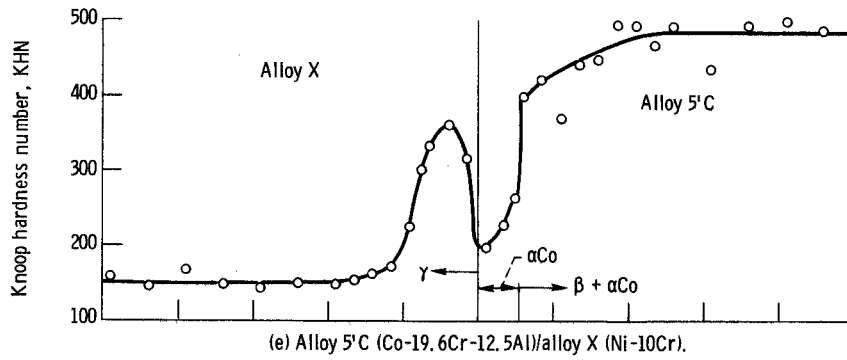
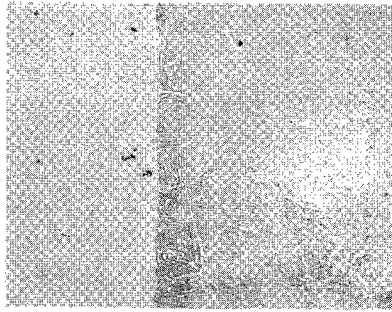


Figure 7. - Continued.

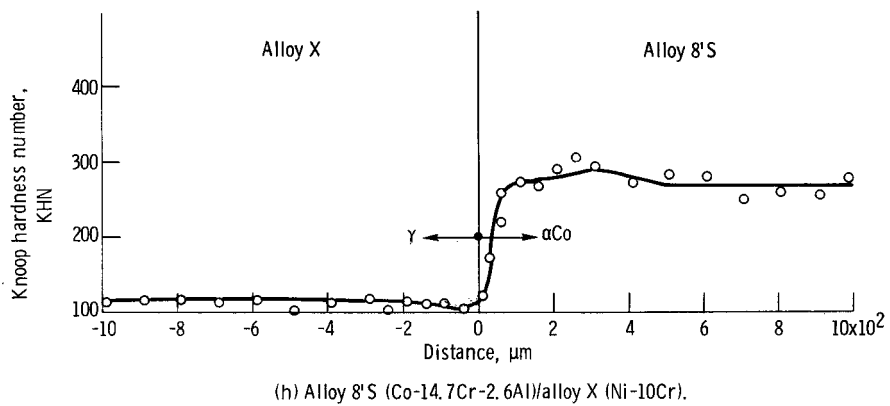
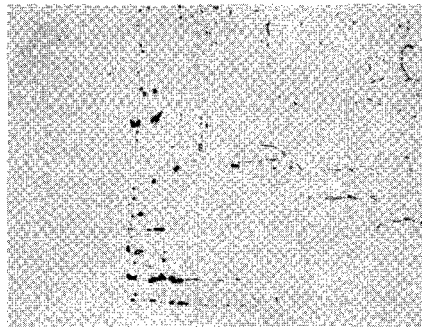
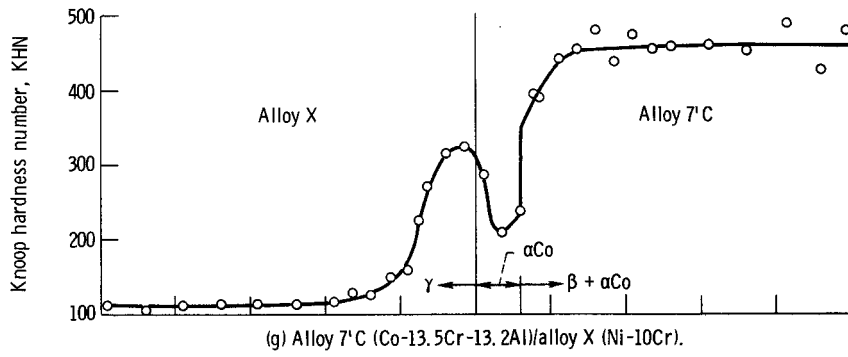
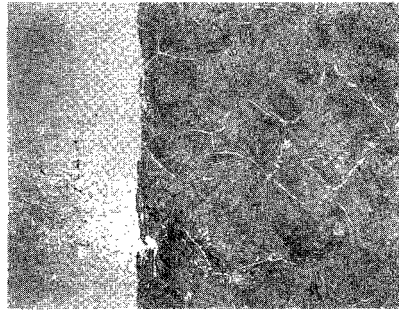
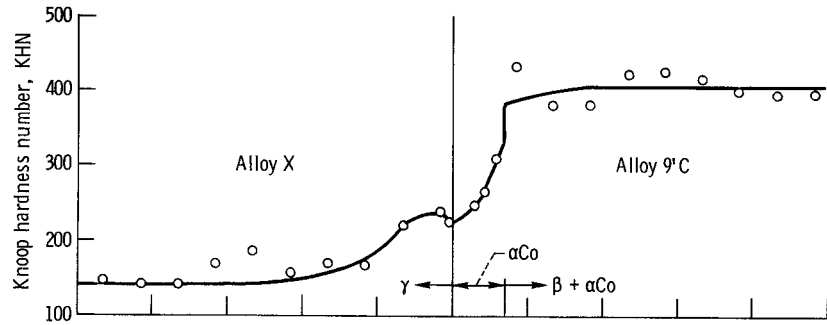
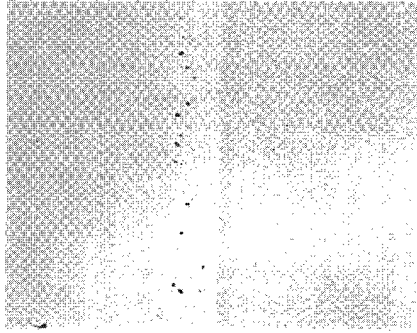
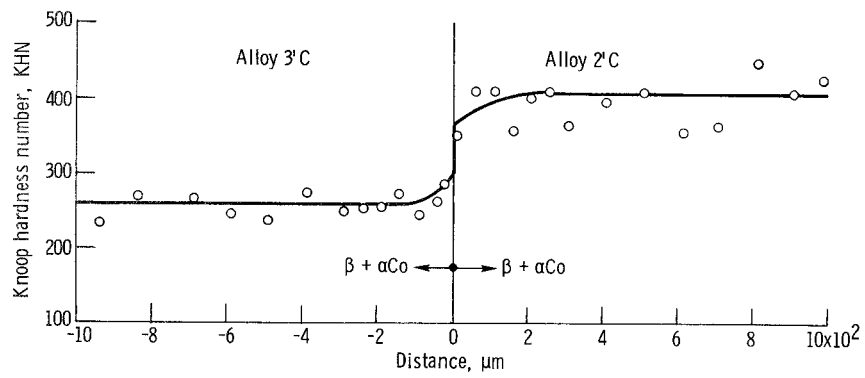
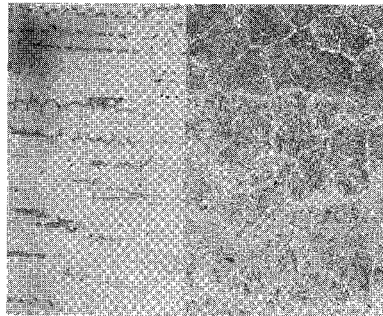


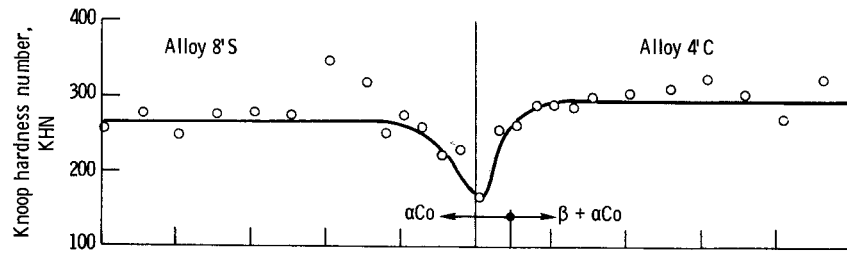
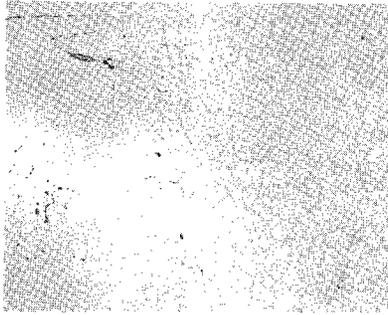
Figure 7. - Continued.



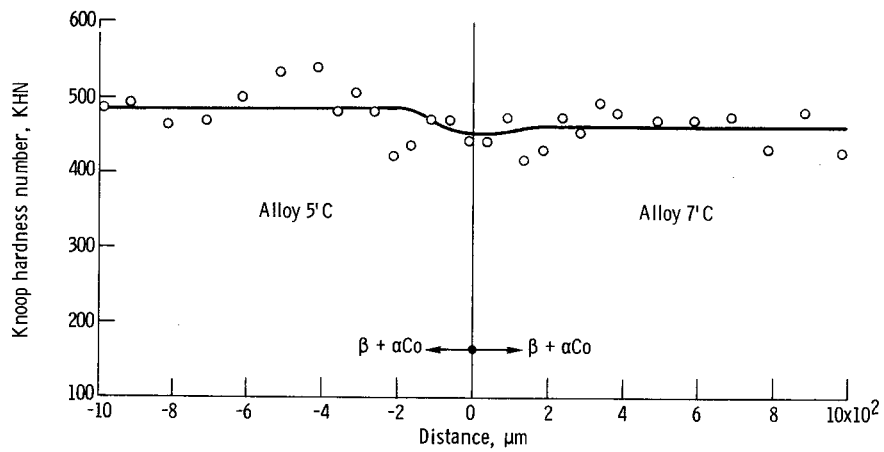
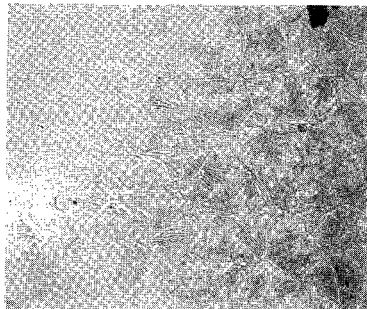
(i) Alloy 9'C (Co-22.1Cr-8.8Al)/alloy X (Ni-10Cr).



(j) Alloy 2'C (Co-11.7Cr-11.0Al)/alloy 3'C (Co-12.3Cr-6.0Al).



(k) Alloy 4'C (Co-18.1Cr-5.8Al)/alloy 8'S (Co-14.7Cr-2.6Al).



(l) Alloy 7'C (Co-13.5Cr-13.2Al)/alloy 5'C (Co-19.6Cr-12.5Al).

Figure 7. - Continued.

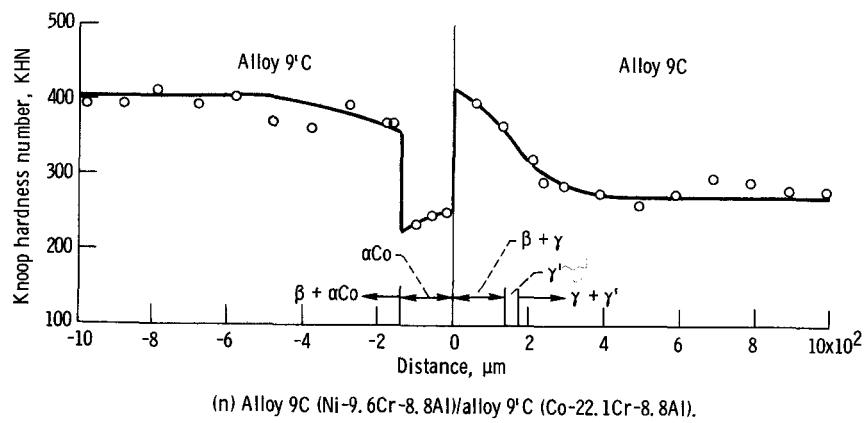
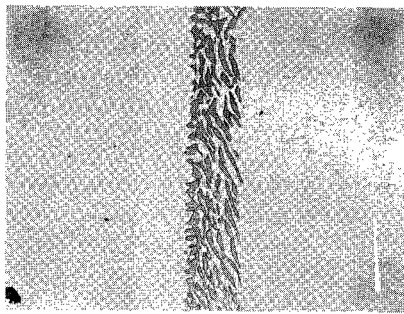
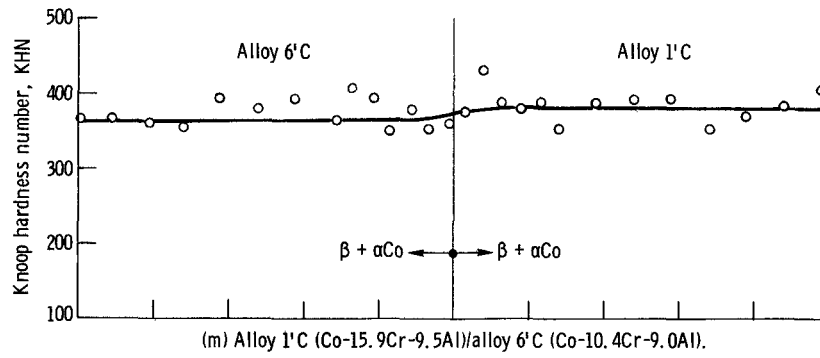
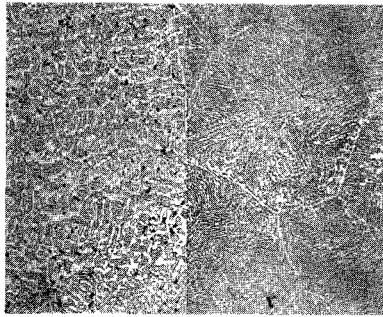


Figure 7. - Concluded.

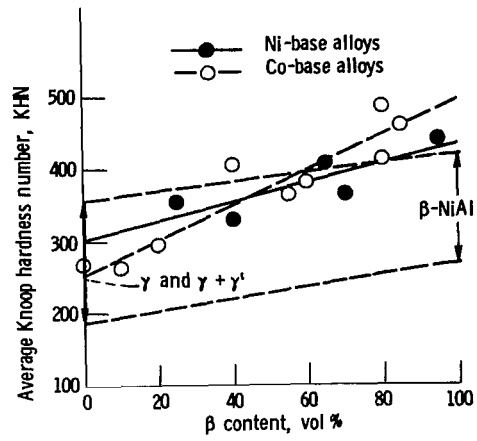


Figure 8. - Knoop microhardness as function of β content in nickel- and cobalt-base MCrAl alloys. (Measurements made on alloys annealed for 500 hr at 1095° C and air cooled.)

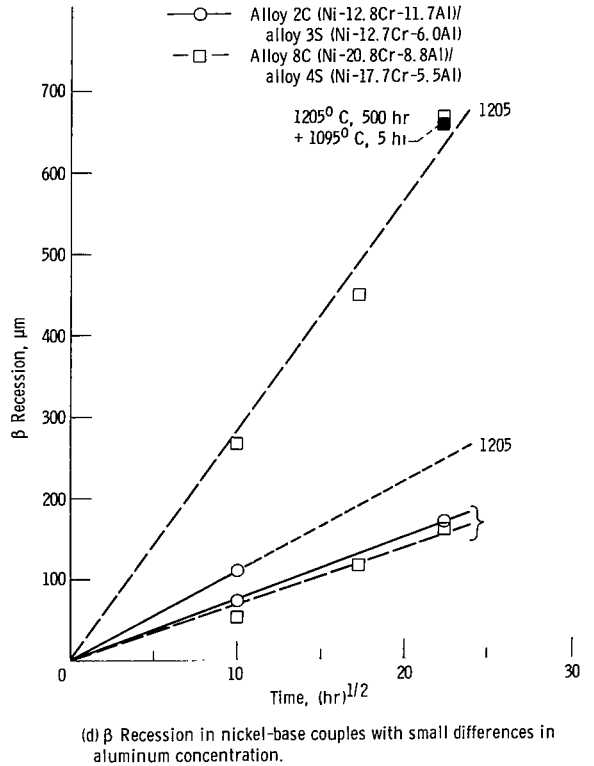
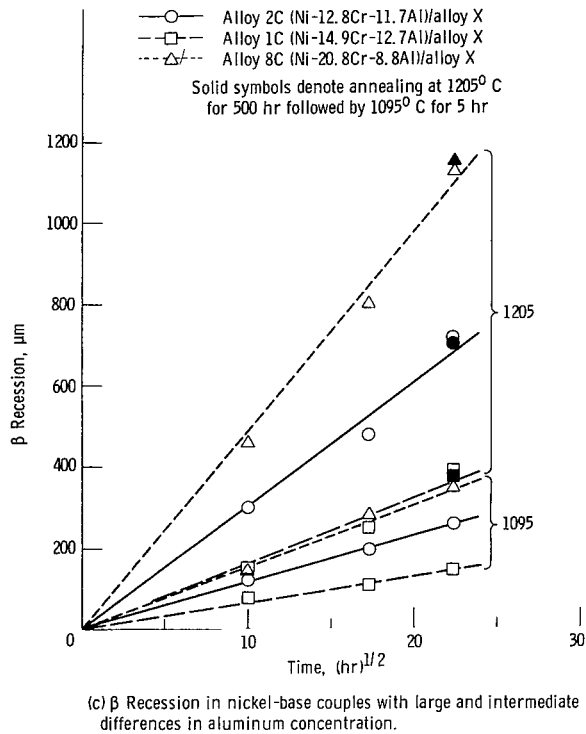
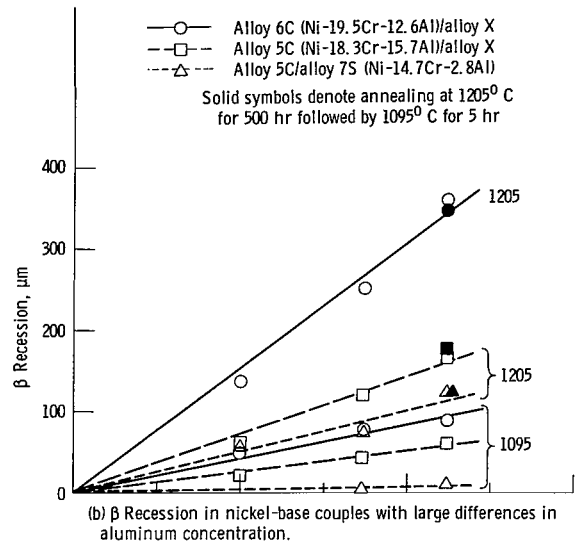
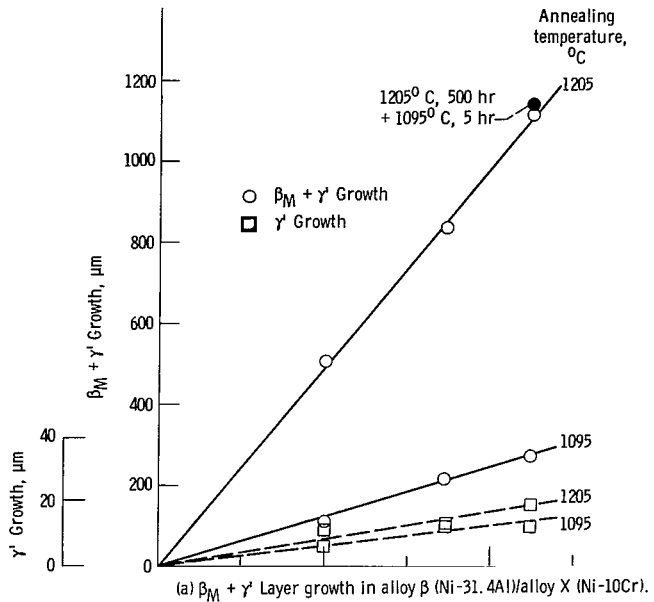


Figure 9. - Layer growth and recession in nickel-base alloy couples.

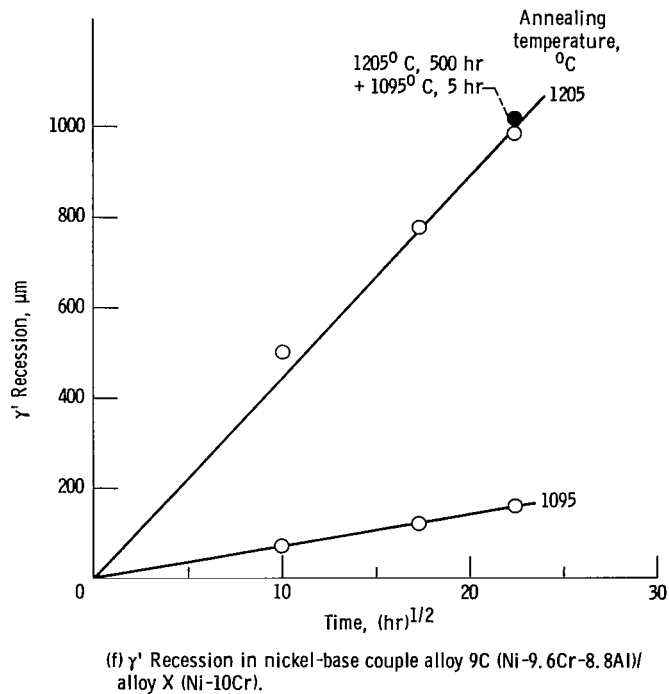
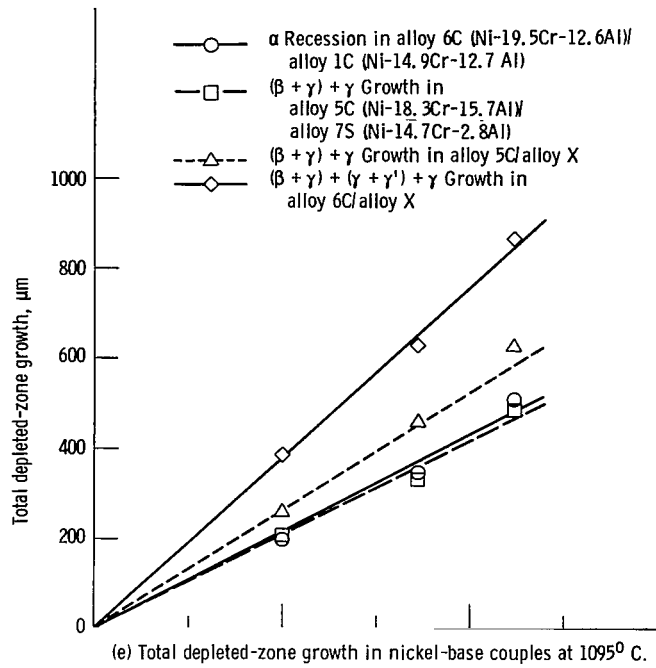


Figure 9. - Concluded.

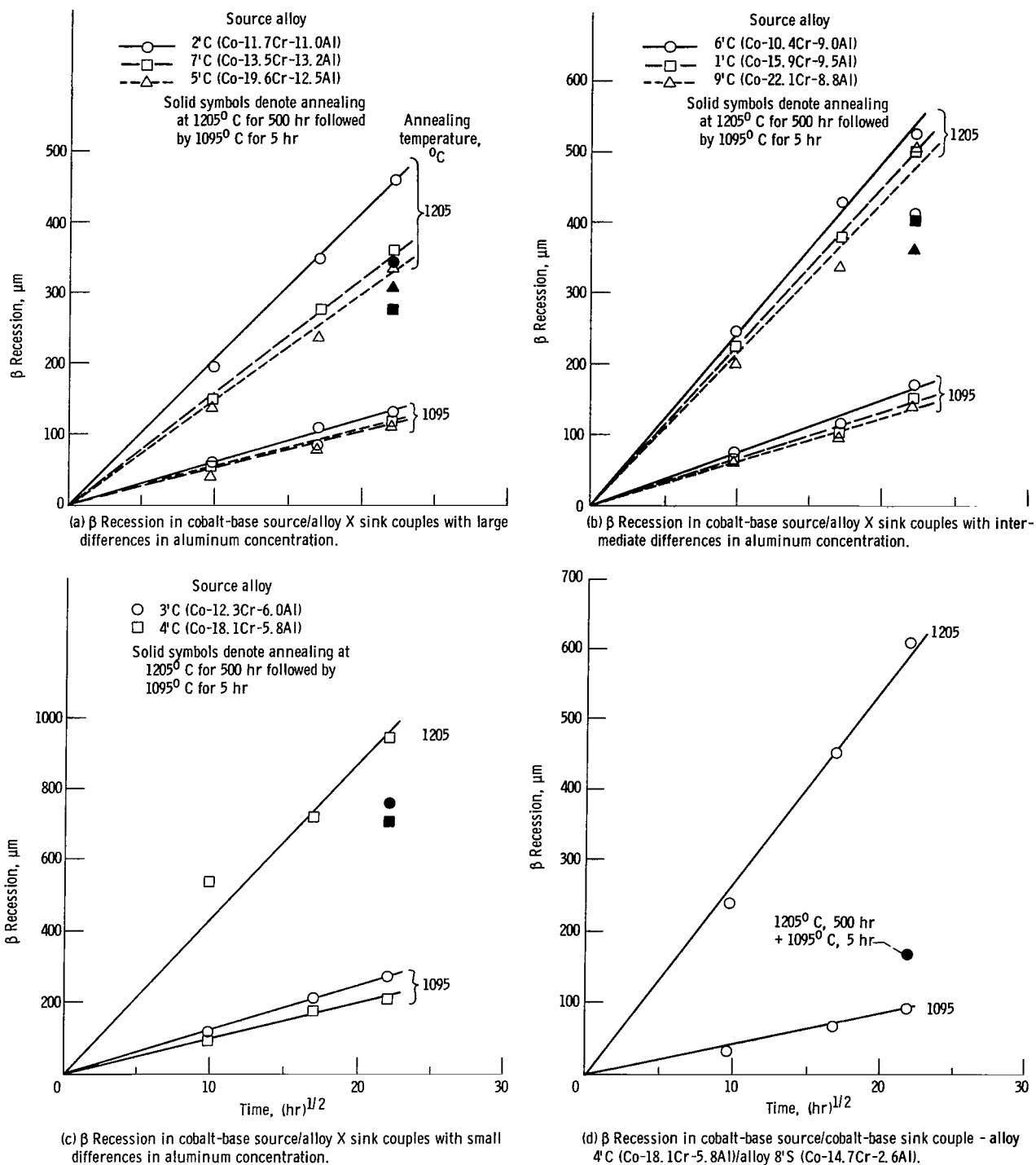
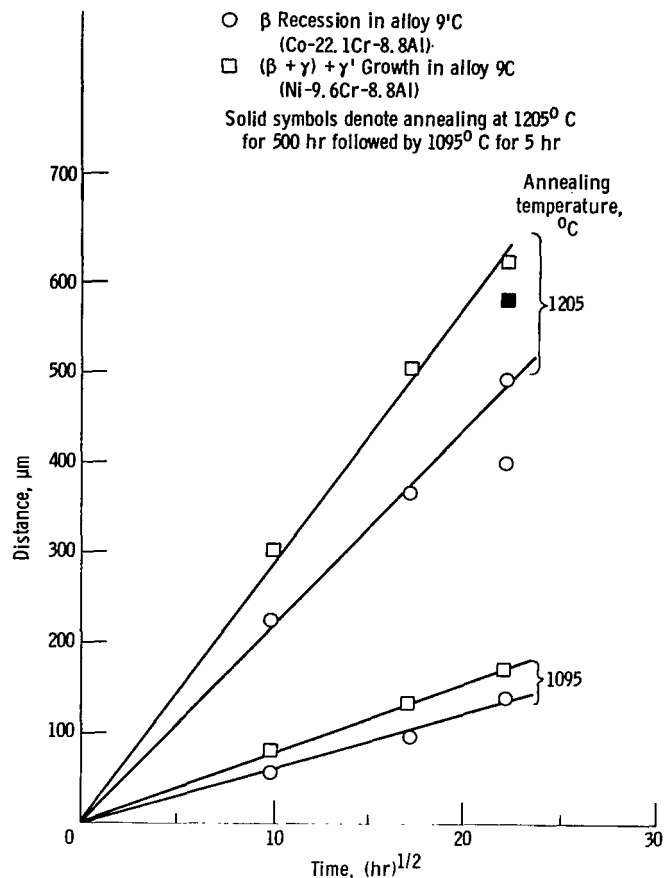
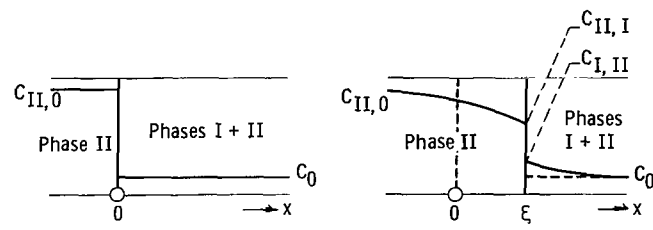


Figure 10. - Layer growth and recession in cobalt-base alloy couples.



(e) Reactions in a cobalt-base/nickel-base couple with source and sink having equal aluminum contents.

Figure 10. - Concluded.



(a) Concentration in phase II ($x < 0$) and in conglomerate of phases I and II ($x > 0$) for time $t = 0$.

(b) Concentration in phase II ($x < \xi$) and in conglomerate of phases I and II ($x > \xi$) at time $t > 0$.

Figure 11. - Diffusion in two-phase system. (From ref. 15.)

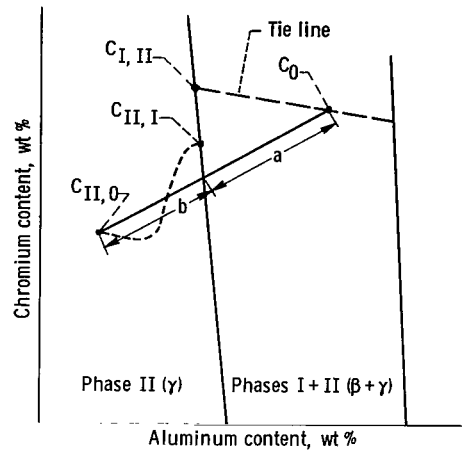


Figure 12. - Relation between Wagner's definition of driving force and β source strength. Driving force (Wagner): $Z = (C_{II, 0} - C_{II, I}) / (C_{II, I} - C_0) \approx b/a$.
 β Source strength: $B = a / (a + b) \approx 1 / (1 + Z)$.

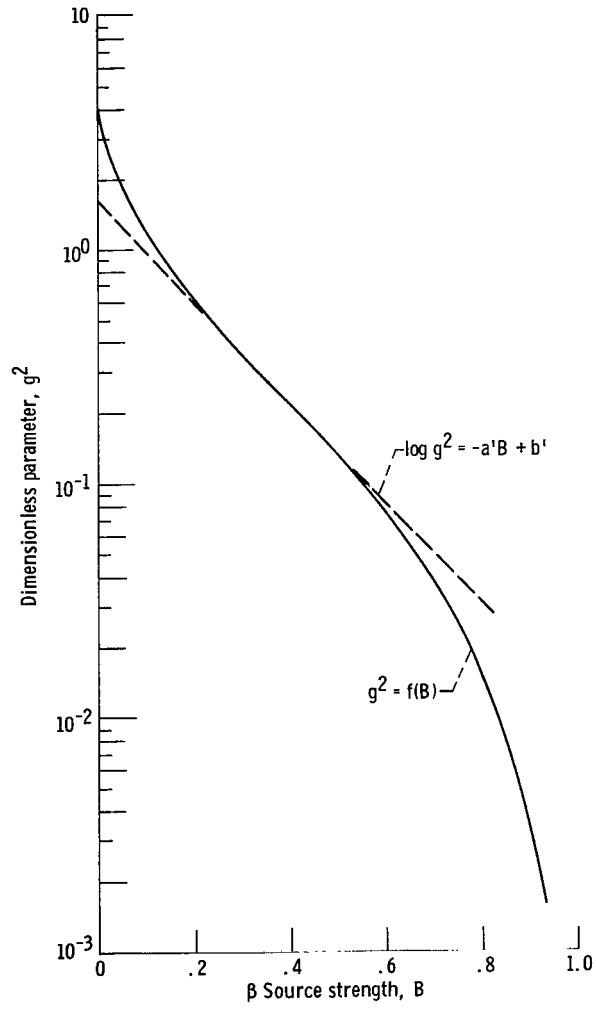


Figure 13. - Dimensionless parameter g^2 as function of β source strength.

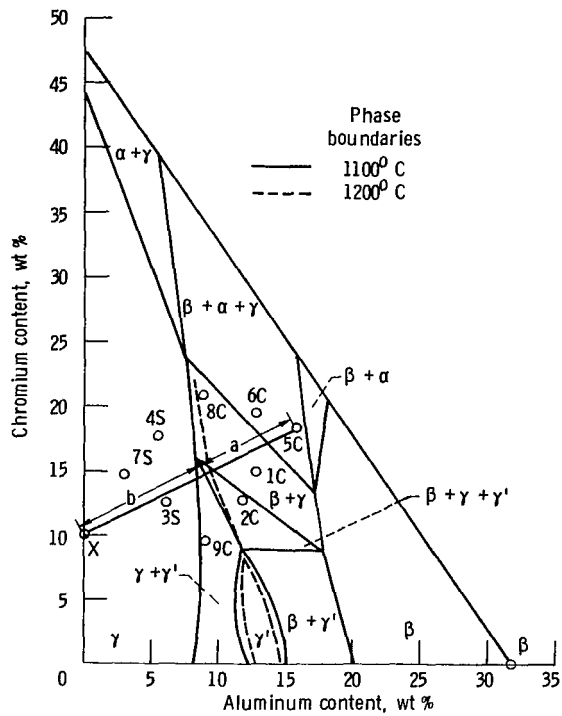


Figure 14. - Estimated 1100^o C and partial 1200^o C Ni-Cr-Al phase diagram showing alloy compositions and method for determining β source strength. (For couple 5C/X at 1100^o C, β source strength equals $a/(a+b)$.)

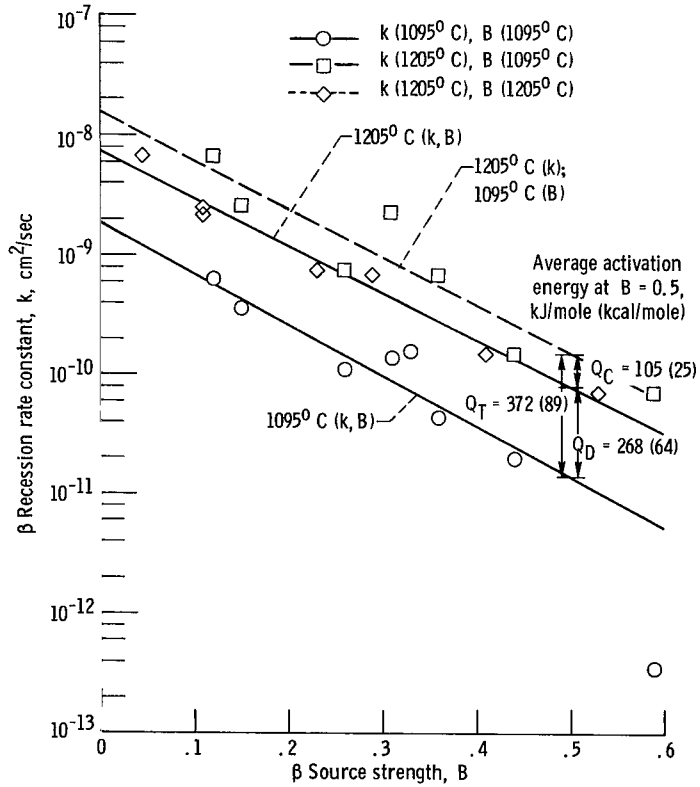


Figure 15. - Correlation of β recession rate constant with β source strength for nickel-base alloy couples.

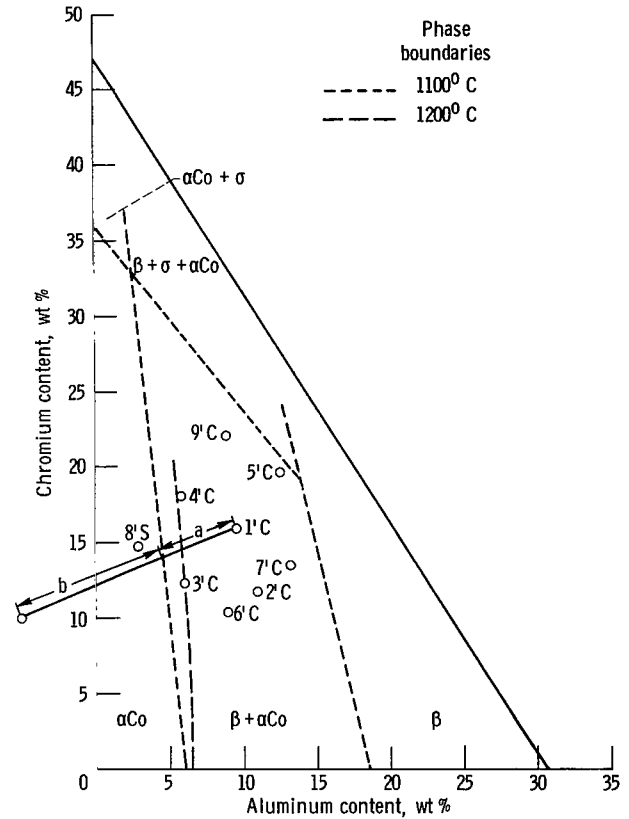


Figure 16. - Estimated 1100 C Co-Cr-Al phase diagram showing alloy compositions studied and method for determining β source strength. (For couple 1' C/X, β source strength equals $a/(a + b)$. The estimated $\alpha\text{Co}/\beta + \alpha\text{Co}$ 1200 C phase boundary is also shown.)

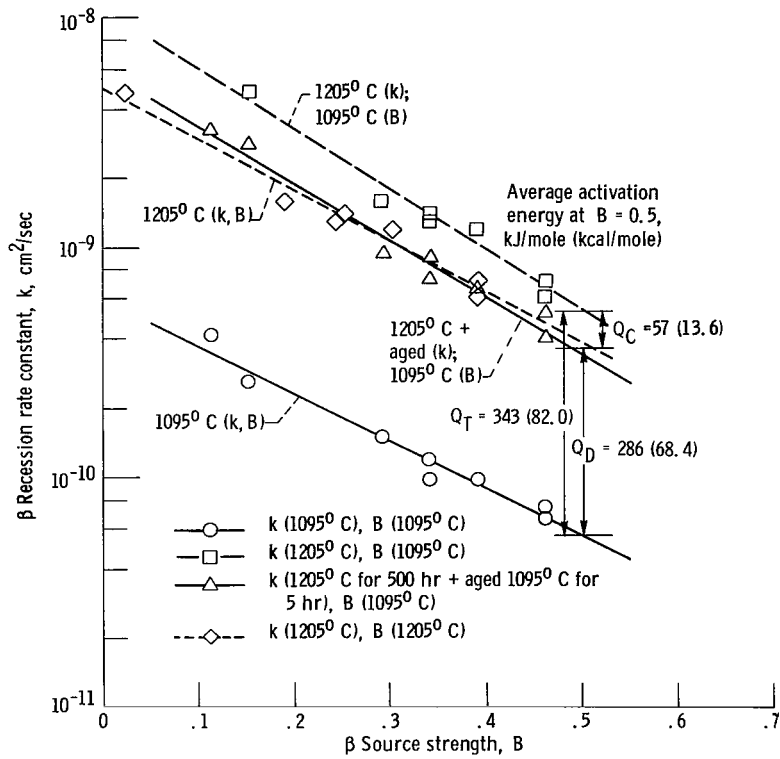


Figure 17. - Correlation of β recession rate constant with β source strength for cobalt-base source/nickel-base sink couples.



079 001 C1 U C 770128 S00903DS
DEPT OF THE AIR FORCE
AF WEAPONS LABORATORY
ATTN: TECHNICAL LIBRARY (SUL)
KIRTLAND AFB NM 87117

POSTMASTER: If Undeliverable (Section 158
Postal Manual) Do Not Return

"The aeronautical and space activities of the United States shall be conducted so as to contribute . . . to the expansion of human knowledge of phenomena in the atmosphere and space. The Administration shall provide for the widest practicable and appropriate dissemination of information concerning its activities and the results thereof."

—NATIONAL AERONAUTICS AND SPACE ACT OF 1958

NASA SCIENTIFIC AND TECHNICAL PUBLICATIONS

TECHNICAL REPORTS: Scientific and technical information considered important, complete, and a lasting contribution to existing knowledge.

TECHNICAL NOTES: Information less broad in scope but nevertheless of importance as a contribution to existing knowledge.

TECHNICAL MEMORANDUMS: Information receiving limited distribution because of preliminary data, security classification, or other reasons. Also includes conference proceedings with either limited or unlimited distribution.

CONTRACTOR REPORTS: Scientific and technical information generated under a NASA contract or grant and considered an important contribution to existing knowledge.

TECHNICAL TRANSLATIONS: Information published in a foreign language considered to merit NASA distribution in English.

SPECIAL PUBLICATIONS: Information derived from or of value to NASA activities. Publications include final reports of major projects, monographs, data compilations, handbooks, sourcebooks, and special bibliographies.

TECHNOLOGY UTILIZATION PUBLICATIONS: Information on technology used by NASA that may be of particular interest in commercial and other non-aerospace applications. Publications include Tech Briefs, Technology Utilization Reports and Technology Surveys.

Details on the availability of these publications may be obtained from:

**SCIENTIFIC AND TECHNICAL INFORMATION OFFICE
NATIONAL AERONAUTICS AND SPACE ADMINISTRATION
Washington, D.C. 20546**